British Geological Survey

Expert | Impartial | Innovative

Measuring soil moisture with spaceborne Synthetic Aperture Radar data

Multihazards and Resilience Programme

Open Report OR/20/004

BRITISH GEOLOGICAL SURVEY

Measuring soil moisture with spaceborne Synthetic Aperture Radar data

A Novellino, M Manosur, L Wang

Keyworth, Nottingham   British Geological Survey   2020

BRITISH GEOLOGICAL SURVEY

The full range of our publications is available from BGS shops at Nottingham, Edinburgh, London and Cardiff (Welsh publications only) see contact details below or shop online at www.geologyshop.com

The London Information Office also maintains a reference collection of BGS publications, including maps, for consultation.

We publish an annual catalogue of our maps and other publications; this catalogue is available online or from any of the BGS shops.

The British Geological Survey carries out the geological survey of Great Britain and Northern Ireland (the latter as an agency service for the government of Northern Ireland), and of the surrounding continental shelf, as well as basic research projects. It also undertakes programmes of technical aid in geology in developing countries.

The British Geological Survey is a component body of UK Research and Innovation.

Foreword

This report is the published product of a study by the British Geological Survey (BGS) supported by the Innovation Flexible Fund (IFF) during the financial years 2018/19 and 2019/20.

The study is part of a much broader programme of assessing the cababilities of satellite data within Earth Sciences conducted by the Geodesy and Earth Observation capability of the Multihazard and Resilience Challenge science area.

Dr Alessandro Novellino has been in charge of compiling and synthesizing the IFF results into a standardized format and writing this report, while Dr Andrew Tye has reviewed and approved the final version of this document.

Acknowledgements

Contents

FIGURES

TABLES

Summary

This report describes the methodology and preliminary results obtained within the NEE6881S Innovation Flexible Fund project funded by the British Geological Survey (BGS) aimed at assessing the capabilities of active radar satellite imagery in deriving soil moisture values.

The first part of the report introduces the project in the context of the most recent methodologies used to assess soil moisture with a particular focus on spaceborne technologies. The second part details the datasets and workflow adopted for the two case studies chosen in this work: Chobham Common and Hollin Hill, both in the UK.

Around 1.7Tb of Synthetic Aperture Radar (SAR) imagery from Senintel-1 satellite have been processed to detect changes of the hydrological conditions at the two sites for the 2015-2018 period. The backscattering coefficient retrieved from Sentinel-1 images has then been compared with ground truth data on the Volumetric Water Content (VWC) and analysed against the ZOODRM recharge model. The main findings are that: the SAR signal has been able to penetrate down to a maximum depth of 15 cm in the terrain (i), the best correlation with the VWC changes is observed with the vertical transmit – vertical receive polarization of the SAR antenna (ii) and for every unit change in the backscatter signal, VWC varies by about 25% to 33% at Chobham Common and ~20% to ~50% at Hollin Hill which translate into a sensitivity of 0.04 dB/[vol.%] to 0.03 dB/[vol.%] and 0.05 dB/[vol.%] to 0.02 dB/[vol.%], respectively.

The Discussion and Conclusions detail the significance and benefits of these findings, current limitations in our methodology and how it can be improved.

1 Introduction

Soil moisture (SM) is the water present in the space between the soil particles and held by means of molecular attraction (Wisler and Brater, 1959). Volumetrically, it is measured as Volumetric Water Content (VWC or θ), namely the ratio of water volume to soil volume in a sample at any given time.

SM is a key environmental variable with a key influence on vegetation health, crop yield, droughts or exposure to flood threats. Therefore knowledge of the spatio-temporal variation of SM is crucial to users in meteorology, climatology, hydrology, hydrogeology, agronomy and civil engineering.

VWC can be measured either in the field or in the laboratory and with different instrumentations:

- Weighing (laboratory)
- Tensiometer
- Electrical resistance
- Time domain reflectometry (TDR) and time-domain transmissometry (TDT), that extract VWC by measuring the dielectric properties of the soil at the punctual locationfollowing calibration with laboratory data.
- Another measurement technique is based on neutron scattering.

All of the technologies discussed above provide a measure of SM in a very small volume of soil (in the order of cubic decimetres), they can be very labour intensive and require many such measures to describe the moisture content across a field. Currently, two non-invasive remote sensing techniques can provide field-scale and regional-scale assessments of SM: ground-based and cosmic ray-based soil sensors (CRS, Figure 1) and microwave sensors carried by satellites, respectively (De Jeu and Dorigo, 2016).

CRS measures naturally occurring neutrons generated by the collision of cosmic rays with the Earth's atmosphere and Earth's surface (Zreda et al., 2008). The neutron count is then corrected for altitude, atmospheric pressure and atmospheric water vapour to account for variations in background cosmic ray intensity and finally calibrated with *in-situ* observations in order to derive VWC (Baatz et al., 2014). The neutron detectors are installed just above the ground, so access tubes are not required, and a single CRS passively measures the neutrons over a footprint of approximatively 350 m in radius (Evans et al., 2016). Starting from 2013 a network of 50 CRS arrays (called COSMOS-UK) has been installed so far across the UK by the Centre for Ecology & Hydrology (CEH or UKCEH) with funding from the Natural Environment Research Council (https://cosmos.ceh.ac.uk/). To perform corrections, calibration and validation of the measurements, CRS stations are surrounded by the following instruments (CEH, 2018): a rain gauge, two TDTs with probes at about 10 cm depth and 2 m apart, profile SM sensors, soil heat flux plate, soil temperature sensors, radiometer, weather station, barometric pressure sensor, temperature and humidity sensor, integrated 2D sonic anemometer, phenocam, snow water equivalent and micrologger.

**Figure 1. Cosmic-Ray Soil Moisture sensor. The photo was taken from
https://cosmos.ceh.ac.uk/network-instruments. Credit: COSMOS-UK, UKCEH.**

According to the CEH, every day the CRS integrates SM over an area up to 200 m in diameter,
and to a depth of up to 70 cm. This framework brings both practical and logistical advantages and
dramatically increases the potential of SM monitoring, because the CRS can be deployed in the
field unattended, for long-term or semi-permanent installations, and provides daily records of SM
over years.

Compared with ground-based sensors, microwave satellites can derive SM from active (radar) or passive (radiometer) microwave sensors. Usually, the former compared to the latter provides better revisiting time (daily or sub-daily vs ~a week) but at coarser resolution (km vs m).

Recent technological advances in satellite remote sensing have produced active radar satellites capable of repeat and accurate observations of SM at almost global scale with much greater resolution than standard radiometers.

However, the calibration of these instruments for SM is still at its infancy especially in temperate climate settings where changes in SM are smaller compared to arid or Mediterranean climates (Bauer-Marschallinger et al., 2018) and the presence of canopy can prevent having a clear radar backscatter signal from the soil.

In this work, we have used the freely-available Sentinel-1 radar data made available from the European Space Agency (ESA through the Copernicus programme (https://sentinel.esa.int/web/sentinel/missions/sentinel-1). We have analysed the semi-empirical relationships at two sites (Chobham Common and Hollin Hill) between the COSMOS-UK observations and the Sentinel-1 radar acquisitions between February 2015 and September 2018. This study represents the first part in the development of a methodology to obtain VWC from active radar sensors, by assessing the correlation between VWC measured by sensors on the ground and radar data from which a regression analysis has been developed. VWC from CRS data have been analysed by taking into account the presence of runoff at the surface derived from the ZOODRM (Zoom Object-Oriented Distributed Recharge Model distributed groundwater recharge model .(Mansour and Hughes, 2004).

The chosen time interval includes the summer of 2018, when dry and sunny weather dominated the UK from May 2018 through to early August (McCarthy et al., 2019), with the thinking being that the difference between the dry and wet season could be detected more easily.

2 Case study and datasets

Two study areas have been considered in this study: Chobham Common in the South East England region and Hollin Hill in the Yorkshire and the Humber region.

Chobham Common is a flat lowland heath (Rowland et al., 2015) located at an altitude of ~47 m above sea level (Figure 2), here COSMOS-UK measurements started from February 2015. Heath elevation might be as high as 1 m.
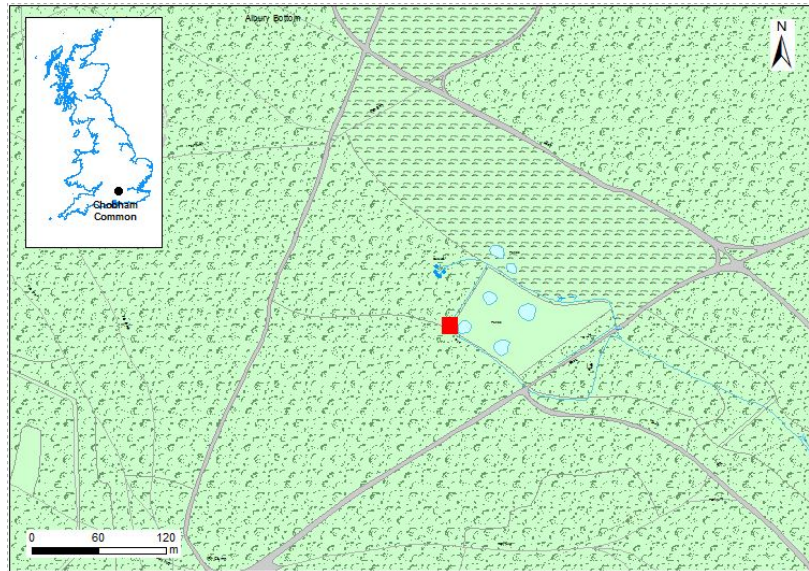
Figure 2 – Location of the Chobham Common site. Contains Ordnance Survey data © Crown copyright and database rights. All rights reserved [2020] Ordnance Survey [100021290 EUL].

Hollin Hill is a grassland site on which sheep graze on a 12 degrees south-facing slope in the Howardian Hills to the north-east of York (Figure 3). Heath elevation might be as high as 1 m. The steepness does not represent the ideal requirements for a COSMOS-UK site and also for radar imagery (due to geometrical distortion issues, see paragraph 2.3) but the site is of interest being one of the BGS landslide observatories (https://www.bgs.ac.uk/landslides/hollinHill.html) where correlation of the landslide motion with increasing shallow moisture dynamics has been proven (Uhlemann et al., 2017). COSMOS-UK measurements started here from March 2014.
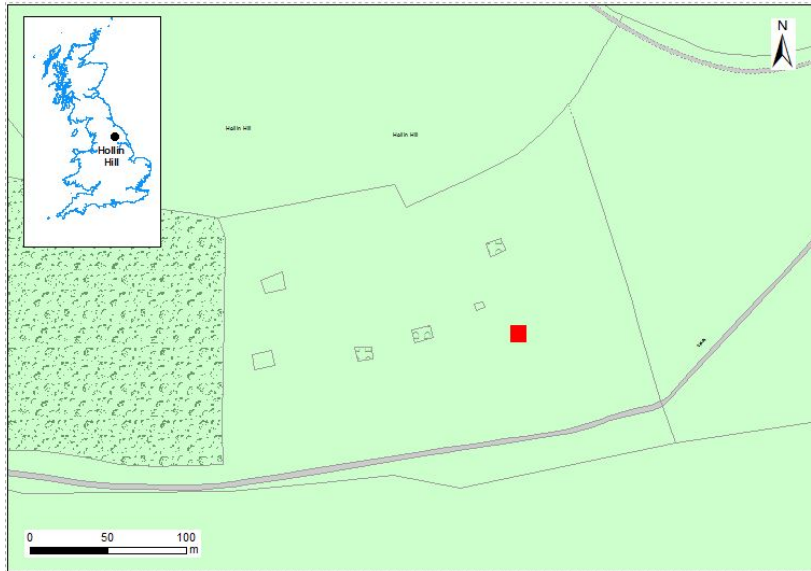
Figure 3 - Location of the Hollin Hill site. Contains Ordnance Survey data © Crown copyright and database rights. All rights reserved [2020] Ordnance Survey [100021290 EUL].

VWC extracted from CRS and precipitation data covers the time of February 2015 – September 2018 for Chobham Common and January 2016 – September 2018 for Hollin Hill.

The time span has been chosen to allow enough VWC observations to provide a baseline reference value against which the effects of Summer 2018 can be verified. The latter being the UK's warmest summer since 2006, the driest since 2003 and the sunniest since 1995 (MetOffice, 2018). This summer significantly impacted VWC at Chobham Common (Figure 4a) and Hollin Hill (Figure 4b) with SM measurements being as low as 20% compared to the VWC minimum of 26/28% of the previous summers.

Peak as high as 60% are recorded for VWC in winter times, much higher than the typical maximum VWC in Mediterranean areas. With VWC > 45%, the soil is expected to be waterlogged and problems may arise in measuring humidity with TDR for example.
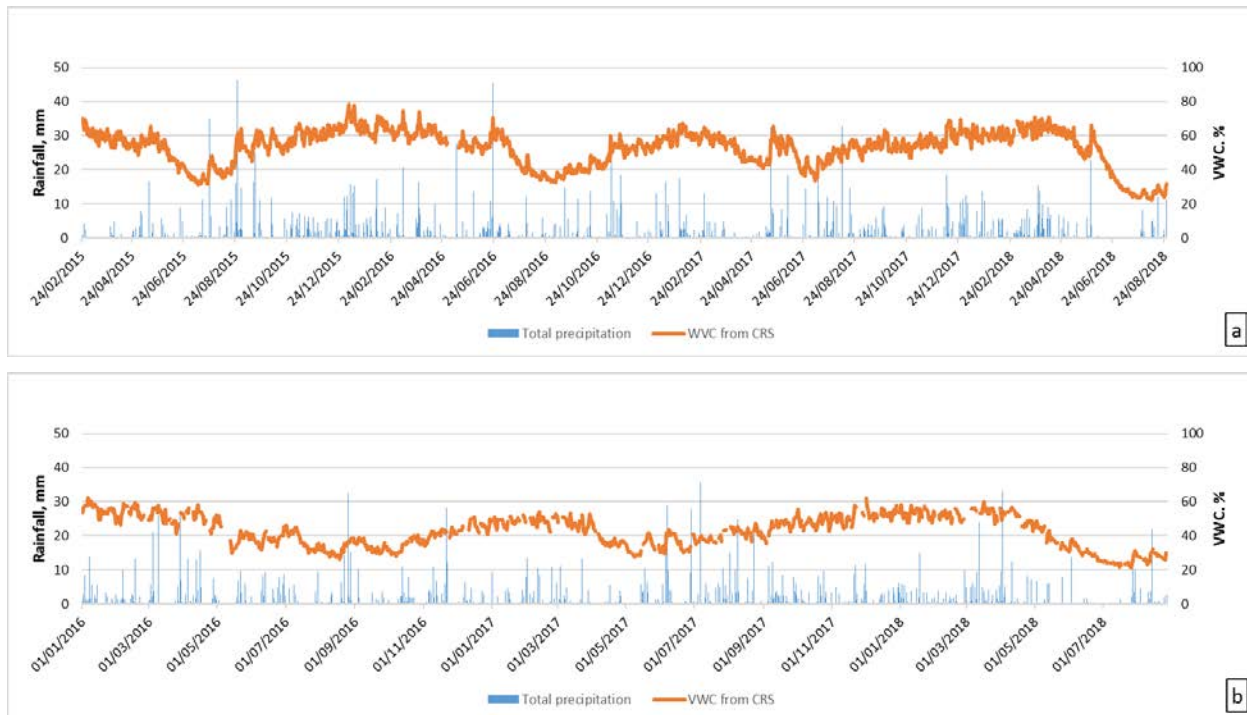
Figure 4 - Rainfall and VWC data for Chobham Common (a) and Hollin Hill (b).

9

2.1 ZOODRM

ZOODRM is a distributed recharge model that was developed at BGS to provide recharge estimates on grids that are compatible with those used by the groundwater model ZOOMQ3D (Jackson and Spink, 2004). ZOODRM is a simple hydrological model that calculates overland flow and recharge at the grid nodes. At each defined location, the model processes rainfall and potential evapotranspiration information and calculates recharge, overland flow (runoff), and soil moisture deficit accounting for the soil characteristics and the land cover type. This model is applied to Great Britain to estimate potential recharge (Mansour et al., 2018).

The calculation of recharge and runoff is based on the approach proposed by Griffith et al. (2006) and is based on the Food and Agriculture Organization of the United Nations (FAO) 56 recharge calculation method. It starts by estimating the total available water (TAW) that can be taken out from the soil store by evapotranspiration. This is calculated as a function of the soil moisture content at field capacity (FC) minus the soil moisture content at wilting point (WP), and the root depth of the plant (Figure 5). This conceptual model relates the evapotranspiration rate to the value of soil moisture deficit (SMD). The SMD is the amount of water taken out of the soil moisture by evapotranspiration. The conceptual model assumes that plants can evapo-transpire at the full potential evaporation rate when SMD is lower than limit called readily available water (RAW). This is calculated as a fraction of TAW. Plants evapo-transpire at a reduced rate if SMD is between RAW and TAW. When the SMD value becomes equal to TAW, no evapotranspiration can occur. During dry periods, the SMD will be always equal to TAW and the plants wilt. During wet periods, rainfall infiltration will fill the deficit in the soil store. If rainfall volume is larger than SMD, the excess water is split into overland flow and recharge using a runoff coefficient (ROC). The runoff coefficient value, which is less than unity, is chosen based on the hydrogeological and topographical characteristics (roughness and slope) at the location where the method is applied. The SMD time series, or alternatively the amount of water stored (soil moisture storage - SMS) in the soil and that can be extracted by plants, is produced at the grid nodes.

The model is run on a daily time step using the daily rainfall and potential evaporation provided by the COSMOS-UK data. A combination of two soil types and two crop types are given to the model as input to investigate the sensitivity of the SMD values to these input data with different combinations. The soil types at Chobham Common and at a location adjacent to it are obtained from the HOST soil data map (Boormann et al., 1995) are used to define the two soil types used in this work. The values of of the soil parameters of these soil types (S1 and S2) are obtained from the work by Griffiths et al. (2008). Table 1 shows the SM content values at field capacity and at wilting points for the two soil types.

The crop type at Chobham Common is grass and this is confirmed by the Land Cover Map LCM2000 (Natural Environment Research Council, 2000). This crop type (P2 in Table 2) is assumed to have a root depth of 0.45 m. In order to ceck the sensitivity of the results to the root depth, a second corp type with a root depth of 0.3 m is also used (crop type P1 in Table 2). Table 2 shows the maximum root depths and the depletion factors set for the two plant types. In all cases, a runoff coefficient value of 1% is used.

Table 1 - Characteristics of the soil data used in the recharge model; values are dimensionless.

Soil type category	Saturation at field capacity	Saturation at wilting point
S1	0.241	0.151
S2	0.235	0.117

Table 2 - Characteristics of the crop types used in the recharge model.

Crop type category	Maximum root depth (m)	Depletion factor (Dimensionless)
P1	0.3	0.64
P2	0.45	0.64

We used ZOODRM outputs to understand the hydrological characteristics of the area at the time of the satellite acquisitions, specifically to assess the occurrence or not of runoff water at the surface.

- Soil parameters moisture content at wilting point (WP) and field capacity (FC).
- Plants maximum root depth (Zr)
- TAW = Zr (FC – WP)
- A depletion factor is used to define the readily available water RAW = dp TAW
- Excess Water = Rainfall – Actual Evaporation – (SMD_{prev} - SMD_{new})
  - for Excess water > 0
    - Potential Rainfall = (1 – ROC) * Excess Water
    - Runoff = ROC * Excess Water
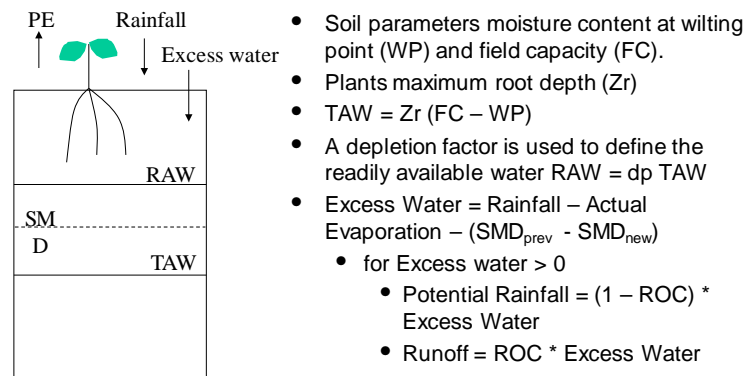
Figure 5 - Overview of the modified FAO recharge calculation method. The abbreviation ROC stands for runoff coefficient.

2.2 SENTINEL-1 PRODUCTS

In both study areas we used Sentinel-1 (S-1) Interferometric Wide (IW) swath mode (De Zan and Guarnieri, 2006), Level-1 Single Look Complex (SLC) products obtained from a Synthetic Aperture Radar (SAR) antenna. These products have been chosen because they represent the main acquisition mode of Sentinel-1 over land, and makes the reproducibility of this work elsewhere easier. The SAR antenna has a central frequency of 5.404 GHz (C-band) corresponding to a wavelength of ~5.5 cm and acquires the signal within an incident angle (θ) range between 29° and 46°. The sensitivity of radar signal to SM decreases with the incidence angle: high sensitivity for low incidences (Baghdadi et al., 2006). At Cobham Common, θ is 37° on the ascending geometry and 39° on the descending one. At Hoolin Hill, θ is 39° on the ascending geometry and 45° on the descending one.

From now on, with the word 'S-1' we refer to the Sentinel-1 IW Level-1 SLC if not specified otherwise. For S-1 data, the SAR antenna supports operation in single polarisation (HH or VV) and dual polarisation (HH+HV or VV+VH), implemented through one transmit chain (switchable to H or V) and two parallel receive chains for H and V polarisation. IW - SLC products contain one image per sub-swath and one per polarisation channel, for a total of three (single polarisation) or six (dual polarisation) images in an IW product. In this work dual polarisation channels (VV+VH), the most common among the available IW products over the UK, have been used.

Each sub-swath image consists of a series of bursts, where each burst has been processed as a separate SLC image and then resampled to a common pixel spacing grid in range and azimuth.

IW - SLC mode generates images with a 250km swath at 2.7/3.5m (along the range direction) by 22m (along the azimuth direction) spatial resolution (ESA, 2016) which are freely accessible through the Copernicus Open Access Hub (https://scihub.copernicus.eu/).

Combining their sun-synchronous trajectory and the Earth's rotation, all SAR satellites revisit the same area two times during one orbit cycle. Therefore, for half of its orbit, the satellite travels from the south pole towards the north pole, the so-called ascending orbit, and, for the other half, from the north pole towards the south pole, the so-called descending orbit. As a consequence, ascending and descending imageries are collected over the same area at different times and, being the satellite side-looking, with different geometries.

Considering the different acquisition geometries and the effects of diurnal variations of the atmosphere on the radar signal propagation, the two satellite geometries have been processed indipendently.

One hundred sixteen S-1 ascending data for the 3/5/2015 – 26/9/2018 period and eighty-seven S-1 descending data for the 12/4/2015 – 29/9/2018 period have been considered for Chobham Common.

Ninety-three S-1 ascending data for the 8/12/2015 – 30/8/2018 period and one hundred seventeen S-1 descending data for the 10/1/2016 – 27/8/2018 period have been considered for Hollin Hill.

3 Methodology

The S-1 images have been processed using the freely available Sentinel Application Platform (also known as SNAP) developed by ESA (available at https://step.esa.int/main/toolboxes/snap/).

In order to extract the final product, the following processing steps have been executed:

- **Apply Orbit file**; during the acquisition of S-1 data, the satellite position is recorded by a Global Navigation Satellite System (GNSS). To assure fast delivery of S-1 products orbit information generated by an on-board navigation solution is stored within the S-1 products. With this step, we consider the refined orbit positions made available later as restituted or precise orbit files by the Copernicus Precise Orbit Determination (POD) Service.

- **Radiometric Calibration**; all S-1 products are not radiometric corrected by default and for the quantitative use of SAR images, a radiometric calibration of radar reflectivity (stored as Digital Numbers) to physical units (radar backscatter) is essential. Otherwise, a comparison of SAR images from different sensors or even the same sensor for different acquisition dates or different acquisition modes is not possible. Backscatter is the portion of the outgoing radar signal that the target redirects directly back towards the radar antenna where it is stored as a complex number. A complex number implies that the representation of a signal, or data file, includes both amplitude and phase values (Figure 6).
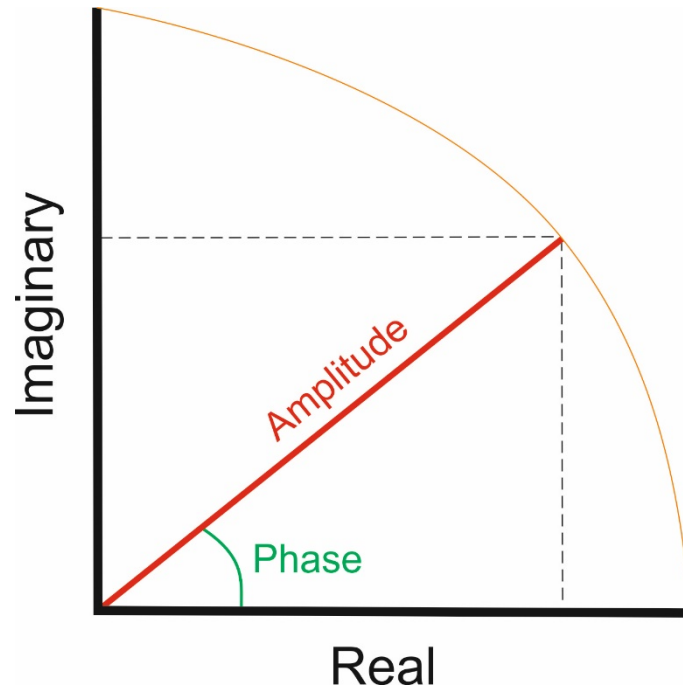
Figure 6 - The radar signal is expressed as a complex number, consisting of a real and imaginary component.

- The scattering cross-section in the direction toward the radar is called the backscattering cross-section (σ) and refers to the intensity (namely amplitude squared) of the backscatter signal. The normalised measure of the radar return from a distributed target is called the backscatter coefficient (σ_0) which is defined as per unit area on the ground and is conventionally expressed in dB units by applying a logarithmic scale (Figure 7).
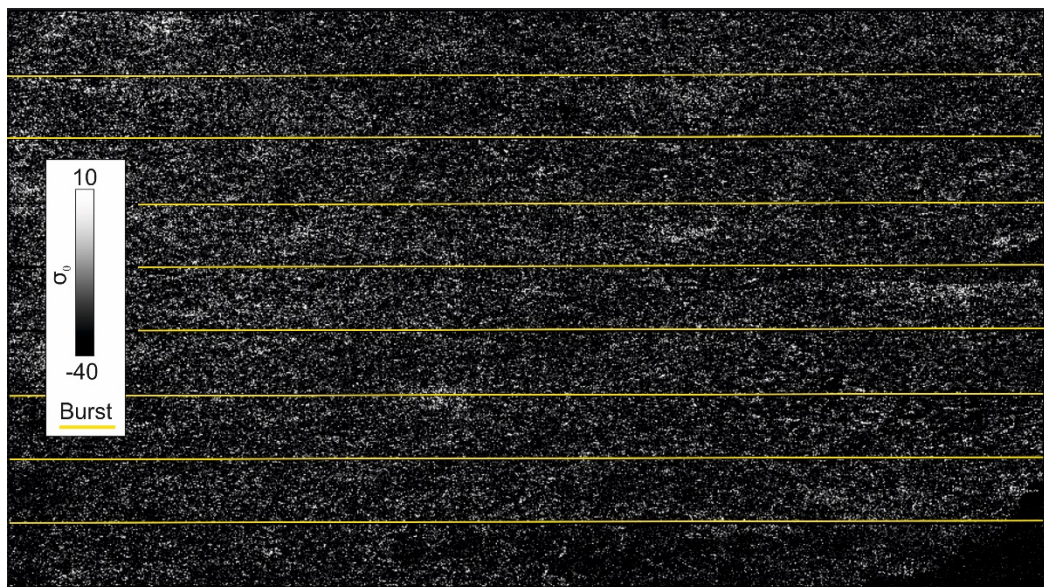
Figure 7 - Sub-swath of S-1 (VV channel) acquired over the Yorkshire region on 25/7/2018. Pixel values expressed as σ_0.

- **TOPSAR-Deburst**; because the different bursts are stored in one single image whereby each burst is separated by a black-filled demarcation, debursting is necessary to combine all the bursts to one single image for each acquisition channel with fluent transitions between the sub-swaths (Figure 8).
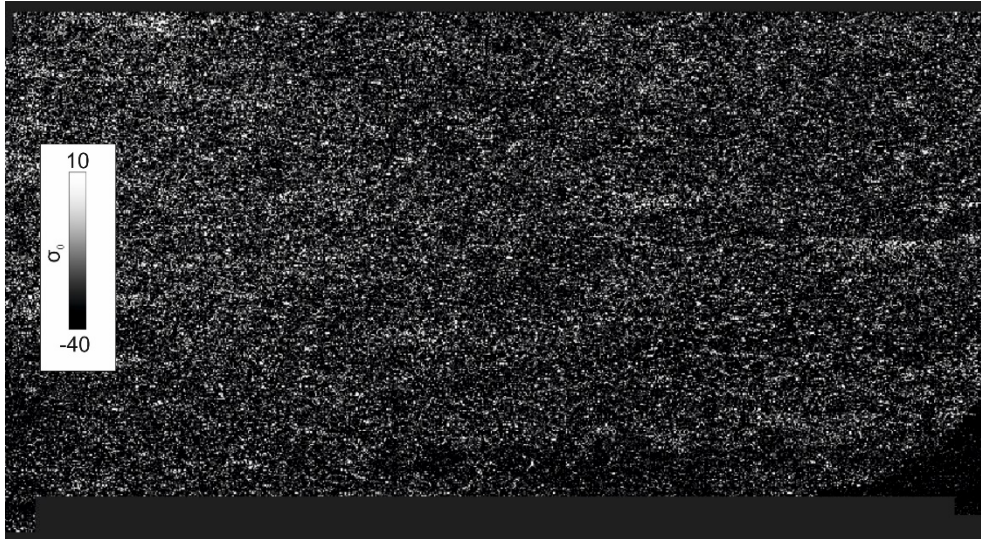
Figure 8 - S-1 (VV channel) acquired over the Yorkshire region on 25/7/2018 after deburst. Pixel values expressed as σ₀ and black filled demarcation have now been removed.

- **Terrain Correction** (also known as **Geometric Correction** or **Range Doppler Terrain Correction**); the geometric correction is undertaken to reduce the distorsion due to the side-looking geometry of the satellite acquisition and to convert the Sentinel-1 SLC data, initially projected in slant range geometry, into a coordinate reference system. By using the 30m SRTM Digital Elevation Model, the topographic effects have been removed and precise geolocation for each pixel of the image has been derived (Figure 9). However, due to the acquisition geometry of the SAR different distortions like foreshortening, layover or shadowing effects still occur (Cigna et al., 2014). The pixel spacing is now ~8 m in range and ~14m in azimuth.
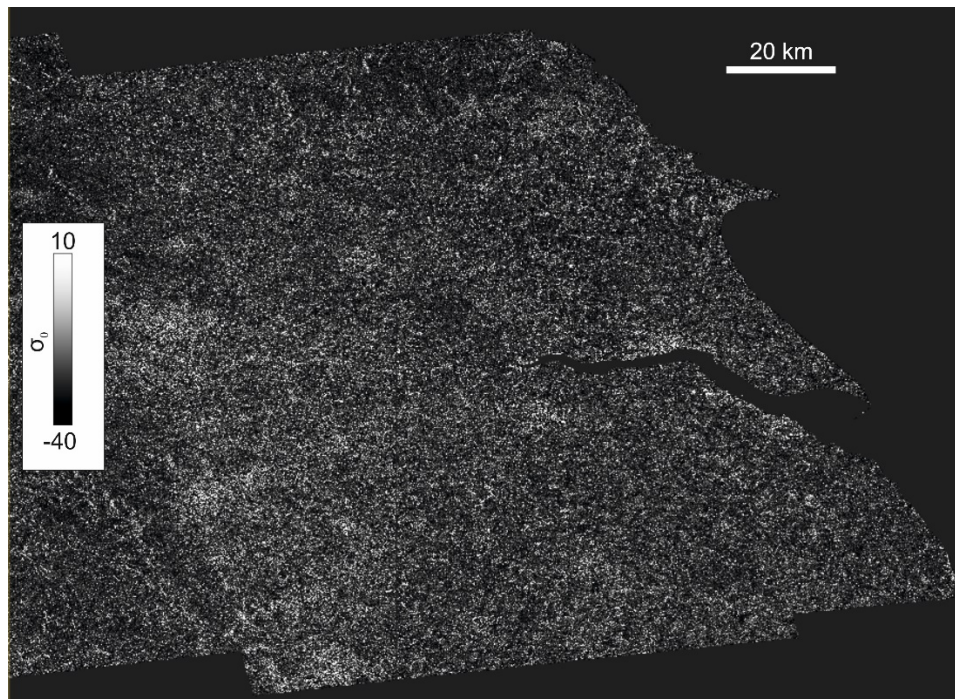
Figure 9 - S-1 (VV channel) acquired over the Yorkshire region on 25/7/2018 after terrain correction.

- **Subset**; the whole image, covering an area of ~45,000 km^2 and with a size of ~4 GB, has been cropped to a much smaller area with an extension of hundreds of km^2 and a size of tens of Mb (Figure 10). This consistently speeds up all the following operations.
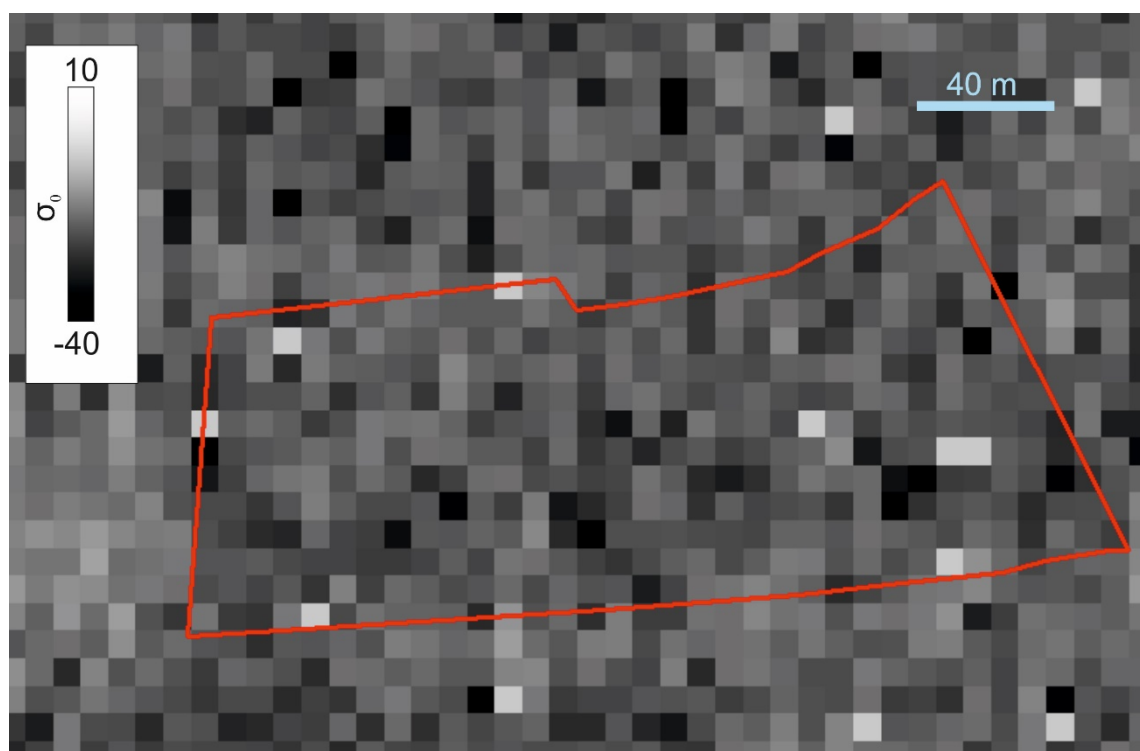
Figure 10 - S-1 (VV channel) acquired over Hollin Hill, delimited by the red polygon, on 25/7/2018 and used to extract σ₀ values.

- **Coregistration**; for enabling a time-series analysis SAR images have to be coregistered. The latter is a method to get every image of the analysed time-series on the same grid system.

- **Export**; the files in the original .dim format are then exported as .tiff files in order to be visualised and analysed in a GIS platform where statistical operations could be performed.

At this stage, σ₀ is controlled by the following physical and geometrical variables of the surface:

- Dielectric constant of the surface (k) which characterizes a given medium's response to the presence of an electric field, in this case, the radar signal. k of a material represents the ratio of its permittivity ε to the permittivity of vacuum ε_0:

$$k = \varepsilon/\varepsilon_0 \qquad (1)$$

- k has a positive relationship with σ₀ and increases in the presence of water (Das and Paul, 2015). Under the same wavelength, permittivity affects the penetration depth of the signal and considering its theoretical relationship with VWC (Koyama et al., 2017), for S-1 the extreme penetration depth ranges between 1 cm during wet conditions and 30cm during dry conditions. Considering the VWC for the analysed period, S-1 data has never penetrated the terrain below 15cm even during the driest periods.

- Terrain morphology respect to the radar incident angle also known as surface roughness. σ_o decreases with the incidence angle (Baghdadi et al., 2016) and in presence of flat surfaces such as water. We have therefore considered also the correlation of σ_o with SMD and SMS values: lowest SMD (corresponding to high SMS) may be indicative of a saturated terrain with occurrence of runoff water at the surface.

- Geometric arrangement of the scatterers, due to the coherent signal emitted by SAR instruments, the disposition of every single scatterer determine the roughness of the surface governs the scattering pattern (see Figure 10). The scattering pattern depends on the polarisation of the wavelength and on the size of the wavelength in relation to the size of the scatterers. Indeed, the main scatterers in an image are the elements having a dimension of the order of the radar wavelength such as vegetation canopy. The latter usually contribuites to the scattering mechanism produced from the terrain or prevents the radar signal to reach the surface at all (Verhoest et al., 2008). In order to reduce or avoid this occurrence, we have therefore chosen two areas with a limited tree coverage where also the Normalized Difference Vegetation Index (NDVI) has been considered. NDVI can provide a clue on the presence of canopy vegetation and vegetation in general affecting the radar signal. NDVI is one of the most widely used vegetation indexes for monitoring vegetation and crop condition (Jiang et al., 2006). Its values range between ±1 with high values related to healthy vegetation grass or forest and low values related to plants under stress or bare soils.

   NDVI values have been interpolated through the whole year starting from the values derived from Sentinel-2 satellite data accessed through the 'Sentinel Hub EO Browser' (https://apps.sentinel-hub.com/eo-browser/).

Because we have used the same sensor and we have compared the two geometries independently over the two sites, the changes in σ_0 are mainly driven by the changes in the dielectric constant of soil and the changes in the geometric arrangement of the individual scatterers inside each pixel during the different seasons. Each of these factors interferes in the microwave reflected and generate what is called the speckle effect, giving the SAR image the typical grainy salt-and-pepper pattern (Chen and Xu, 2014).

All these factors must be considered and corrected if we want to compare images acquired over different passes from the same sensor or also from different sensors.

σ_0 typically ranges from +10 dB for very bright objects to -40 dB for very dark surfaces. Flat surfaces such as calm water normally appear as dark areas in a radar image since most of the incident radar pulses are specularly reflected away (see Figure 9). Trees and other vegetations are usually moderately rough on the C-band wavelength scale. Hence, they appear as moderately bright features in the image with σ_0 ranges from -10 dB to -20 dB. Very bright targets may appear in the image due to the corner-reflector or double-bounce effect where the radar pulse bounces off the horizontal surface towards the target and then reflected from one vertical surface of the target back to the sensor. Examples of such targets are built-up areas, ships on the sea, high-rise buildings and regular metallic objects such as cargo containers.

The extraction of σ_0 and CRS data occurred through the development of scripts in Octave specifically tailored to read data from the COSMO files and the satellite imagery (see Appendix 1).

A total of ~1.7Tb of satellite data has been processed in order to compare, for each site, VWC from CRS with:

- σ_0 in the VV channel derived from the ascending geometry.
- σ_0 in the VH channel derived from the ascending geometry.
- σ_0 in the VV channel derived from the descending geometry.

- σ_0 in the VH channel derived from the descending geometry.

Spatially, we considered the median σ_0 over an area of $\sim 1 \times 10^5$ m^2, encompassing around 600 pixels for Chobham Common and 360 pixels for Hollin Hill.

The chosen area allows to: be consistent with the size of the area affecting the CRS measurement (see Section 1), have uniform landcover within the two sites and reduce the effect of both the speckle noise and the geolocation error, which is ~20 m on our sites. The geolocation error should have been considered and removed in case only the pixel corresponding to the CRS sensor had been taken for the comparison.

Temporally, we started with a raw correlation, where all the σ_0 values have been considered, and then accounted for different thresholds for NDVI and SMS values to remove σ_0 measurements which, for specific dates, might have been affected by the presence of vegetation and runoff water, respectively.

On the NDVI and SMS filtered data, we have also taken into account the different frequency of data collection, so that the correlation has considered not only a comparison between σ_0 and CRS measurments on the same day, as shown in the figures of in Section 4.1 and 4.2, but also:

- Comparison of σ_0 with CRS measurments recorded one, two, three, four and five days after the satellite acquisition.
- Comparison of σ_0 with CRS measurments averaged over two, three, four and five days after the satellite acquisition.

Considering successive or multiple days is based on the assumption that, while satellite measurements are almost instantaneous measurements, the data recorded by the CRS are affected by water content within a volume of terrain where vertical water circulation takes place down to depths sometimes below the penetration capability of the satellite signal. Depending on the time required for this circulation, different VWC values might be recorded by the CRS.

All the combinations together resulted in a total of fourty comparisons.

The comparisons have been assessed through the Pearson correlation coefficient (ρ) between the two populations (X and Y) according to the formula:

$$\rho = \frac{cov\ (X,Y)}{\sigma_X \sigma_Y} \qquad (2)$$

Where cov is the covariance and σ is the standard deviation of the population; ρ values range between +1 and −1, where 1 is a total positive linear correlation, 0 is no linear correlation, and −1 is total negative linear correlation.

The correlation analysis has been followed by a regression analysis on the channel with the highest ρ. The regression is aimed at examining the influence of the independent variable, the VWC, on the dependent variable, σ_0. Dealing with quantitative and continuous variables a linear model has been used and the corresponding sum of squared estimate of errors (SSE) is reported.

4 Results

4.1 CHOBHAM COMMON

For Chobham Common, the SMD values estimated with the recharge model with soil type S2 and the crop type P2 (Grass) are used in the subsequent analysis (Figure 11) . P2 represents a grass crop type with a maximum root depth of 0.45 m and soil S2 has a total available water content (AWC) of 0.118 where AWC is equal to FC minus WP (Table 1 and Table 2). As SMS and soil SMD are two different representations of the same process, which is the availability of water in the soil, their time series are simply opposite to each other and they can be both used as a proxy to soil saturation. It can be seen from Figure 11 that during wet periods, the SMD becomes close to zero, while the SMS reaches the total available water (TAW) calculated by multiplying the root depth by available water content (AWC), which yield in this case a value of 53.1 mm. At this point we might expect water at the surface which alters σ_0 because the dielectric constant has changed, so these dates have been removed from the comparison.

Conversely, during dry periods, the SMD reaches the highest value, which is the same value of total available water (TAW), while the SMS reduces to zero. Under this condition, the reflecting surface is represented by the terrain with the NDVI providing clues on the presence or not of vegetation.

CRS data are sharply decreasing following the dry Summer 2018 and display a delay of some weeks with precipitation overall.
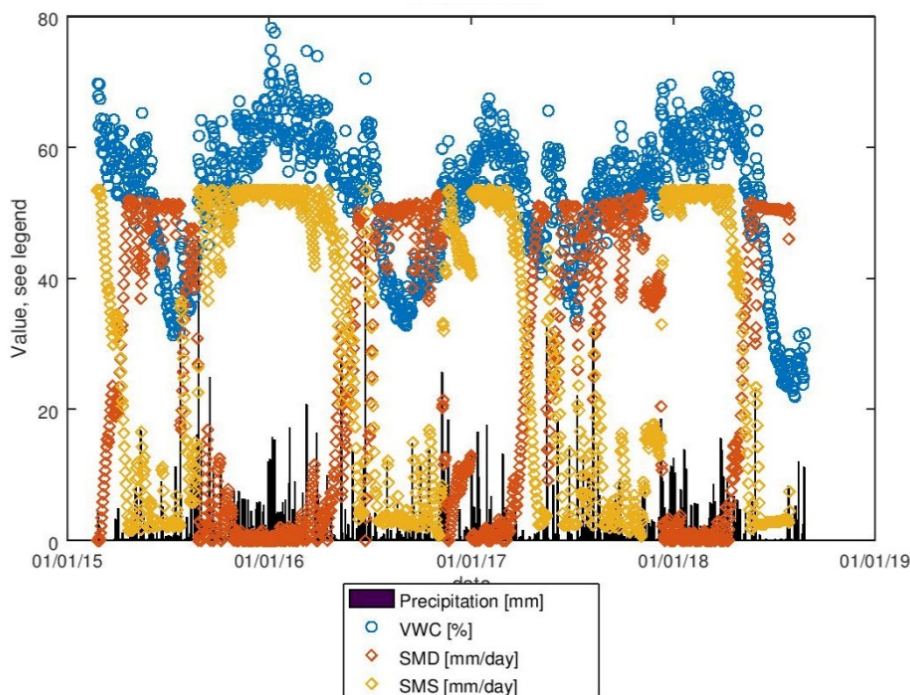
Figure 11 - Relationship among rainfall, TDTs, VWC measured by the CRS and SMS and SMD modelled by ZOODRM for Chobham Common.

Figure 11 shows that there is a time consistency between the reduction of the CRS-VWC and the increase of the SMD (or the reduction of SMS). However, it is clear that rate of reduction of SMD is much higher than the rate of the VWC measured by the CRS. This could be caused by the fact that the conceptual model the recharge model is based upon is not fully compatible with the processes taking place within the penetration depth limits of the CRS that typically range between 15 and 40 cm. For example the recharge model calculates the increase of SMD as a direct result of evapo-tranpiration stresses exerted by the plants and that rainfall is the only source of water that

compensate for SMD. The CRS is measuring, on the other hand, the SM content within the top of the soil and this is impacted by additional processes such as the occurrence of the dew point and other atmospheric and biological processes that maintain SM for longer period of times. The recovery of the CRS-VWC looks much smoother than the recovery of the soil storage and that could be to the same reasons explained before, for example a small amount of rainfall may start up the recovery process at the top of the soil as shown by the CRS measurements, while in the recharge model this rainfall amount may get completely lost to evapotranspiration and no clear recovery is apparent until significant volume of precipitation occurs. This reflects the different vertical scale the recharge model and the CRS measurements are based on.

The same-day measurements obtained from COSMOS-UK data and σ_0 from the two channels of the S-1 ascending geometry are shown in Figure 12. The standard deviation of the VV channel is lower than the one from the VH channel (0.72 dB vs 0.76 dB).

Figure 12 - Correlation between VWC extracted from CRS and σ_0 of the VH and VV channels for S-1 ascending data over Chobham Common.

For the ascending geometry, among all the fourty combinations, the correlation coefficient is always higher for the VV channel rather than VH (Appendix 2).

We found that ≤0.6 for NDVI and ≤50 mm/day for SMS, were the best empirical thresholds and, when applied, they always increase ρ by removing the outliers.

The best ρ (0.74) is observed with the filtered VV when the CRS values are averaged over three days starting from the satellite acquisition day (included).

With a SSE of 13.33dB, the linear regression model for the highest ρ is represented by the following equation:

19

$$VWC = \frac{\sigma_0 + 15.26}{0.04} \qquad (3)$$

Equation (3) means that for every dB of σ_0 VWC can range of ~25% which translates into a sensitivity of 0.04 dB/VWC.

The same-day measurements obtained from COSMOS-UK data and σ_0 from the two channels of the S-1 descending geometry are shown in Figure 13. The standard deviation of the VV channel is lower than the one from the VH channel (0.74 dB vs 0.92 dB).

Figure 13 - Correlation between VWC extracted from CRS and σ_0 of the VH and VV channels for S-1 descending data over Chobham Common.

As for the ascending geometry, among all the fourty combinations, the correlation coefficient is always higher for the VV channel rather than VH (Appendix 2). However, the descending correlations are consistently lower than those found in the ascending geometry.

We found that ≤0.5 for NDVI and ≤50 mm/day for SMS were the best empirical thresholds even if, when applied, they only improve ρ for the VV channel.

The best ρ (0.55) is observed with the filtered VV when the CRS values are averaged over two days starting from the satellite acquisition day (included).

With a SSE of 17 dB, the linear regression model for the highest ρ is represented by the following equation:

$$VWC = \frac{\sigma_0 + 15.56}{0.03} \qquad (4)$$

Equation (4) means that for every dB of σ_0 VWC can range of ~33% which translates into a sensitivity of 0.03 dB/VWC%.

Equations (3) and (4) show that when the shallow soil is completely dry, namely VWC is 0, σ_0 is ~=-15 dB at Chobham Common.

4.2 HOLLIN HILL

For Hollin Hill, the SMD and SMS values are calculated from a recharge model with soil type S1 and crop type P1 (Figure 14). P1 represents a crop type with a maximum root depth of 0.3 m and S1 has an AWC of 0.09 (Table 1 and Table 2).

Temporally, the same correlations of Chobham Common between SMS, SMD, CRS and precipitation are found in Hollin Hill (Figure 14).
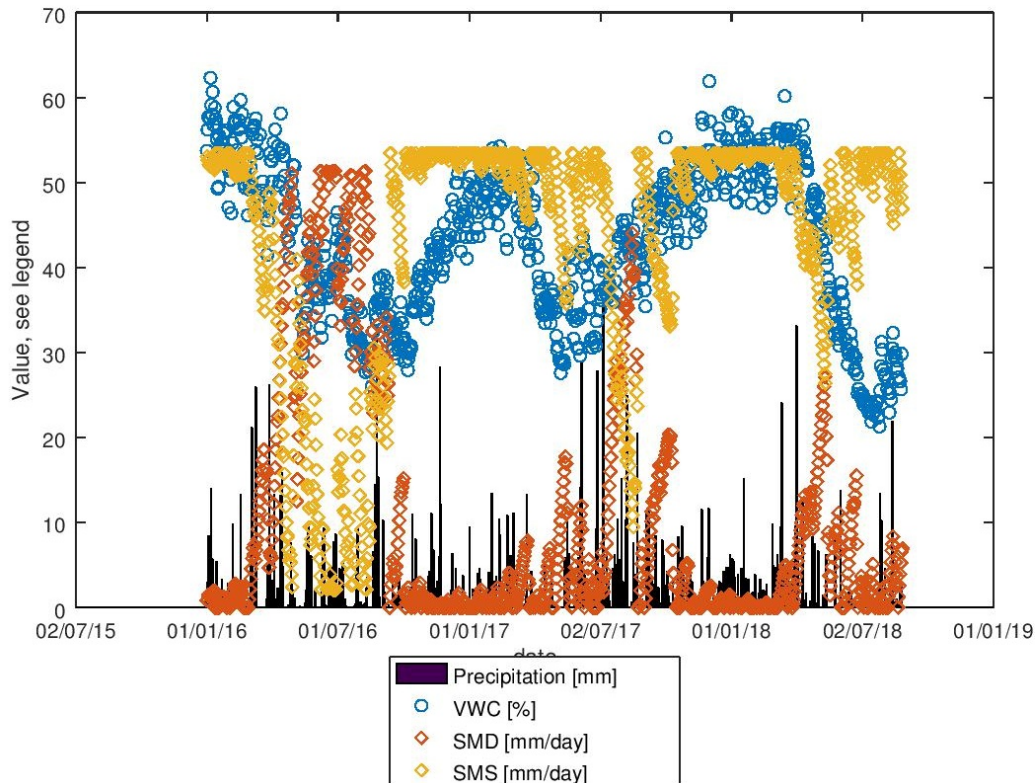
Figure 14 - Relationship among rainfall, TDTs, VWC measured by the CRS and SMS and SMD modelled by ZOODRM for Hollin Hill.

Figure 14 shows the same differences in behaviour between the recorded CRS-VWC values and the simulated SMS values. It is clear that the fluctuations of the VWC are much smoother than the fluctuations of the SMS or SMD and this is due to deficiencies in the conceptual model the recharge is based on as explained in Section 4.1.

The same-day measurements obtained from COSMOS-UK data and σ_0 from the two channels of the S-1 ascending geometry are shown in Figure 15. The standard deviation of the VV channel is slightly higher than the one from the VH channel (0.98 dB vs 0.9 dB).
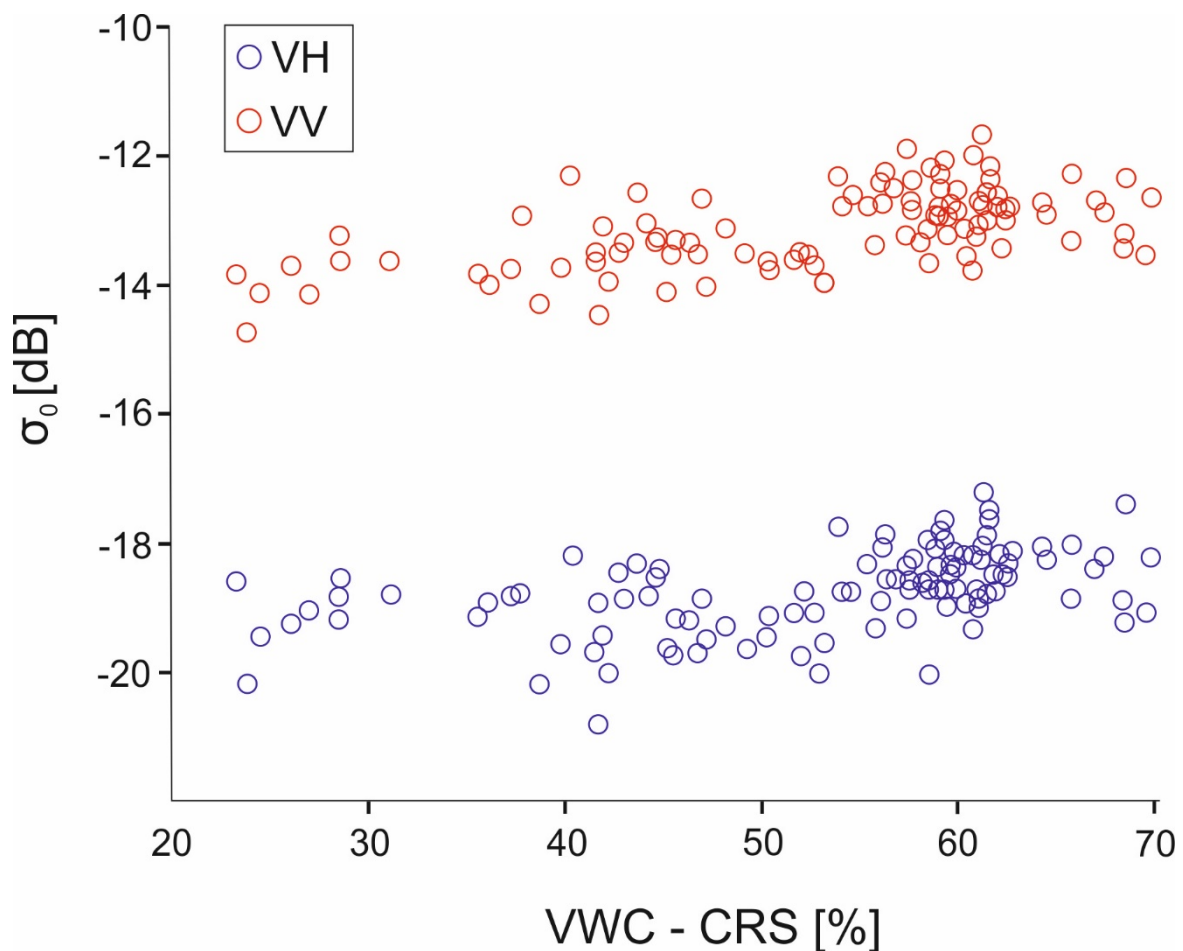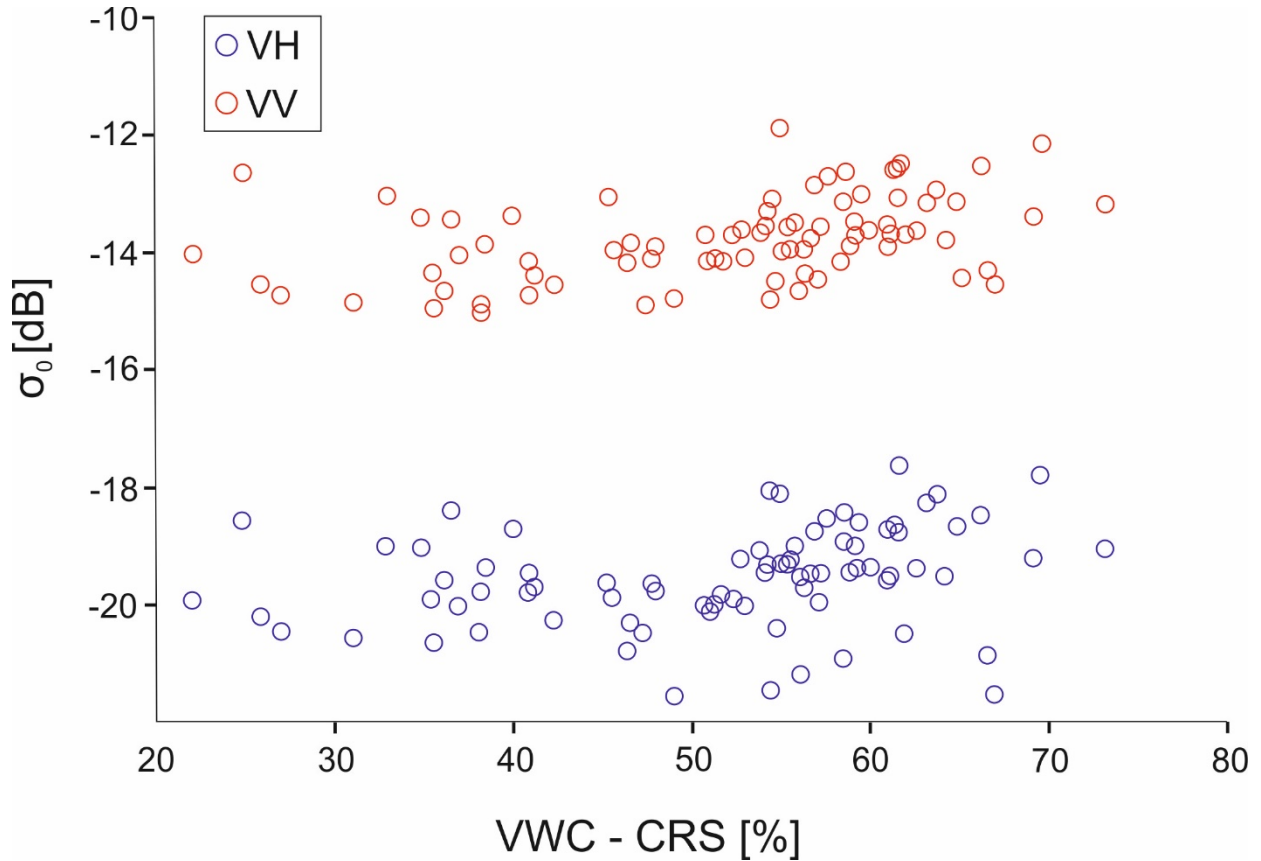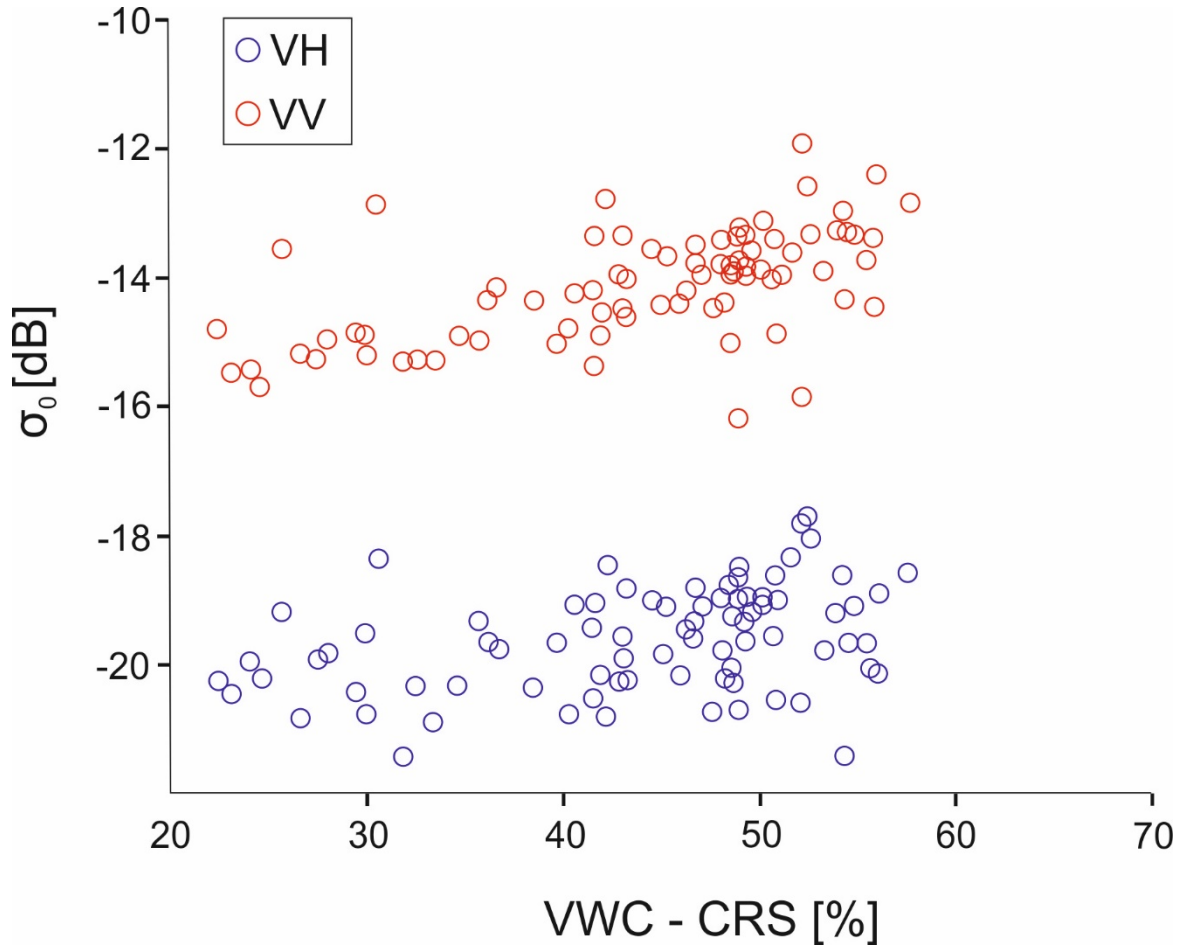
Figure 15 - Correlation between VWC extracted from CRS and σ$_0$ of the VH and VV channels for S-1 ascending data over Hollin Hill.

For the ascending geometry, among all the fourty combinations, the correlation coefficient is always higher for the VV channel rather than VH (Appendix 2).

We found that not always the NDVI and SMS empirical thresholds were able to improve the correlations (Appendix 2).

The best ρ (0.58) is observed with the filtered VV when the CRS values are averaged over four days starting from the satellite acquisition day (included).

With a SSE of 21.24 dB, the linear regression model for the highest ρ is represented by the following equation:

$$VWC = \frac{\sigma_0 + 16.92}{0.05} \qquad (5)$$

Equation (5) means that for every dB of σ$_0$ VWC can range of ~20% which translates into a sensitivity of 0.05 dB/VWC.

The same-day measurements obtained from COSMOS-UK data and σ$_0$ from the two channels of the S-1 descending geometry are shown in Figure 15. The standard deviation of the VV channel is slightly higher than the one from the VH channel (1.19 dB vs 1.13 dB).
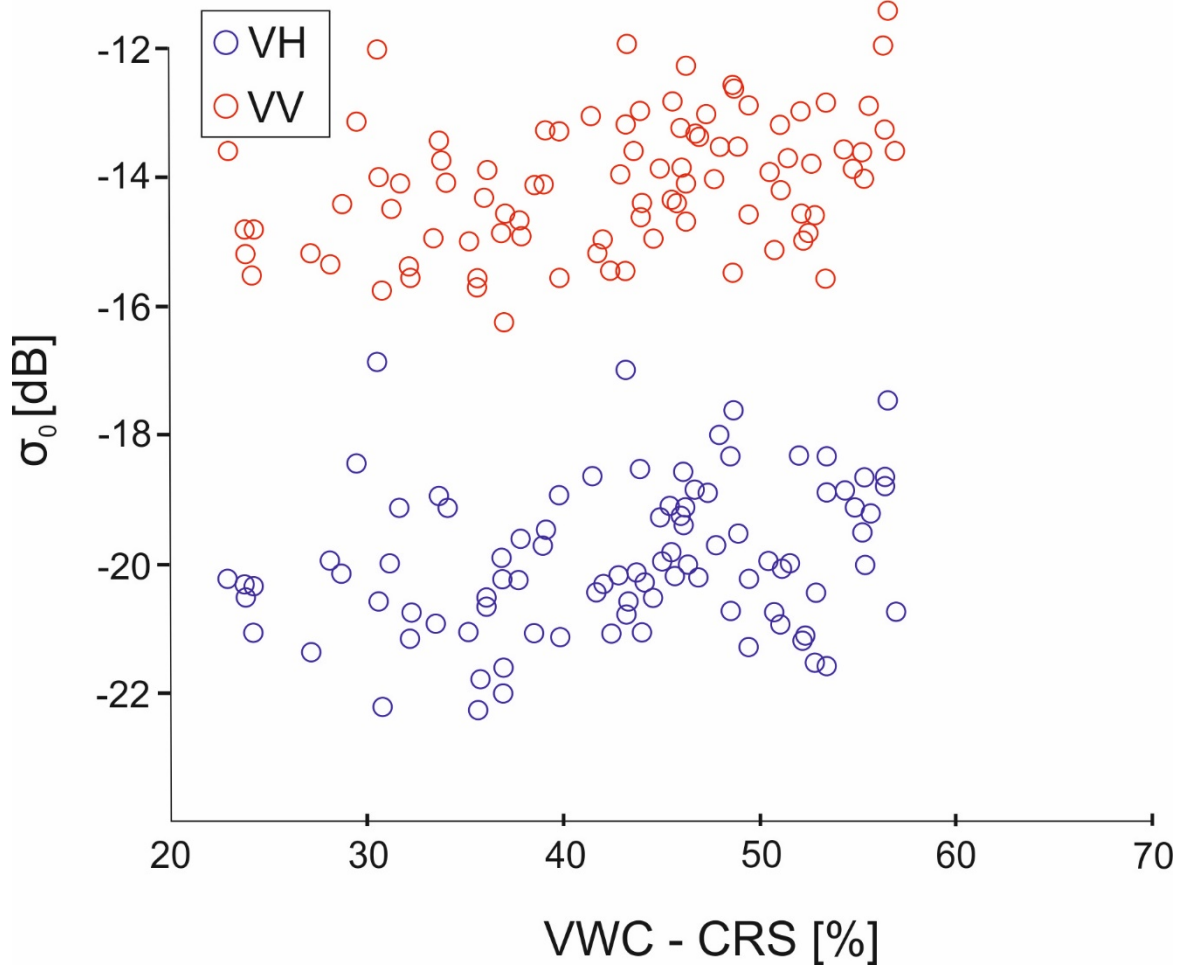
Figure 16 - Correlation between VWC extracted from CRS and σ₀ of the VH and VV channels for S-1 descending data over Hollin Hill.

Differently from the previous results, the best correlation coefficient for the descending geometry is not always associated to the VV channel (Appendix 2).

We found that NDVI and SMS empirical thresholds do actually decrease the correlations (Appendix 2).

The best ρ (0.39) is observed with the unfiltered VV when the CRS values are averaged over five days starting from the satellite acquisition day (included).

With a SSE of 30.3 dB, the linear regression model for the highest ρ is represented by the following equation:

$$VWC = \frac{\sigma_0 + 15.91}{0.02} \qquad (6)$$

Equation (6) means that for every dB of σ₀ VWC can range of ~50% which translates into a sensitivity of 0.02 dB/(VWC%).

Equations (5) and (6) show that when the shallow soil is completely dry, namely VWC is 0, for this type of terrain σ₀ is ~=-16/17 dB at Hollin Hill.

Compared to Chobham Common, higher SSE in Hollin Hill might be explained by the geometrical distorsions (foreshortening effect) occurring on this slope, especially over the S-1 descending geometry (Novellino et al., 2017). This finding confirms that high radar incident angles compared to the slope angle cannot be used to derive VWC.

5 Discussion and Conclusions

SM is an indispensable input data for hydrology. Due to the fact that the collection of in situ SM data in remote areas is often impractical or impossible, the development of alternative data collection method is necessary.

This report investigates the estimation of surface VWC using Sentinel-1 satellite for use in hydrological applications and its potential for estimating VWC in the UK climate setting. This preliminary study has allowed developing scripts to automatically extract data from the input datasets (COSMOS-UK records and radar imagery) to be used for analysing the correlation.

Additionally, this work is the first analysis of the correlation between σ_0 and the VWC extracted by the COSMOS-UK datasets.

From this preliminary investigation the following conclusions can be already derived:

- CRS values can effectively represent changes in VWC as proven by the ZOODRM model.
- Considering the groundwater recharge model rates of changes, the results suggest that CRS and σ_0 are both measuring VWC in the top soil at depths shallower than 15 cm.
- Regardless of the area and the geometry used, VV always represents the best channel for the correlation between σ_0 and VWC derived from CRS. NDVI thresholding has a great influence in ρ but it does not always improve the correlation.
- For the period analysed, for every unit change in σ_0, VWC varies from 25% to 33% at Chobham Common and from 20% to 50% at Hollin Hill.

Despite the correlation is documented and always detected over the two sites and for the two geometries, ρ is lower than the values reported from literature and derived from linear model which can be as high as 0.9 (e.g., Alexakis et al., 2017).

Our results can be affected by the fact that soil humidity has been so high during the wettest periods, with VWC $\geq$50%, that water can be at surface and erase any possibility to associate σ_o with VWC. At these conditions, we begin to have problems measuring humidity with TDR for example and, in addition, the radar signal instead of increasing with humidity may start to decrease being reflected away.

Therefore further analyses are required to translate satellite remote sensing input from VV to VWC with the following activities to be considered:

- Disentangle dielectric constant from all the other components affecting σ_0 such as the terrain morphology and the geometric arrangement of the scatterers.
- Considering, for each site, a different size of the area from which σ_0 values are extracted taking into account the variogram of σ_0 to account for the variability of the radar signal.
- A dynamic filtering for NDVI.
- Using a different data mining method, like machine learning techniques, to derive the regression model and to consider also the different penetration depth of σ_0 through time. Indeed, time lags between σ_0 and CRS due to movements of water in the soil column have been detected. These may affect the signal recorded by S-1 as the radar signal might have recorded a VWC at shallower or deeper depth than the CRS measurement.

Appendix 1

Octave programming language has been used in this work. Through this appendix, Octave scripts to be run on the commands line are in blue, lines within each script are in *Italic*, comments are in brown, entries that are specific to the input data being processed and require modification are in red and outputs are in green.

There are two main steps: extracting COSMOS-UK measurements and ZOODRM modelled data (1) and find the correlation with σ_0 (2).

Here we are going to show the analysis done for the SAR ascending acquisitions over the Chobham Common site. Similar scripts have been written for the descending acquisitions and for the Hollin Hill site.

'SAR_soil_moisture_ChobhamCommon_ascending.m' refers to step 1 and 'post_processing.m' to step 2.

SAR_soil_moisture_ChobhamCommon_ascending.m

#this script will only create a single files where COSMOS data, sigma0, SMS and SMD are all collected together over the same day

format long g

#move to the working directory

cd   'C:\Users\alessn\Desktop\projects   and   proposals\KE_fellowship\Innovation   Flexible Fund\COSMOS_data\ChobhamCommon_Reading';

output_directory='C:\Users\alessn\Desktop\projects   and   proposals\KE_fellowship\Innovation Flexible Fund\COSMOS_data\ChobhamCommon_Reading';

#read input file from the COSMOS table only for the SAR dates we have

range='A1:A10000'; #the S-1 asc dates, you can go further below the number of rows to be sure you have taken everything!

dates_asc=xlsread('CHOBH-2015-02-24-2018-08-27_buffer2-mean_median.xlsx','SAR_sigma0_asc',range); dates_asc2=dates_asc-1;

dates_asc3=datestr(dates_asc2,'dd/mm/20yy'); clear dates_asc dates_asc2

#extract the COSMOS dates

range='A7:A10000'; #the COSMOS dates

dates_cosmos=xlsread('CHOBH-2015-02-24-2018-08-27_buffer2-mean_median.xlsx','CHOBH-2015-02-24-2018-08-27',range); dates_cosmos2=dates_cosmos-1;

dates_cosmos3=datestr(dates_cosmos2,'dd/mm/20yy'); clear dates_cosmos dates_cosmos2

#take the daily precipitations starting from the previous month before the first SAR acquisition and ending at the last SAR date

```
range='A2:A20000';  #the SMD and SMS dates

dates_SMS=xlsread('ChobhamCommon_SMD_and_SMS.xlsx','Plot_SMD',range);
dates_SMS2=datestr(dates_SMS,'dd/mm/yy'); dates_SMS3=cellstr(cell(size(dates_SMS2),10));

if str2num(dates_SMS2(1,7:8))<89
    dates_SMS=dates_SMS-1;
    dates_SMS2=datestr(dates_SMS,'dd/mm/yy');
end

dates_SMS3=cellstr(cell(size(dates_SMS2),10));
if str2num(dates_SMS2(1,7:8))>89
    for i=1:size(dates_SMS,1)
        if i<=3652
            dates_SMS3{i}=strcat(dates_SMS2(i,1:6),'19',dates_SMS2(i,7:8));
        else
            dates_SMS3{i}=strcat(dates_SMS2(i,1:6),'20',dates_SMS2(i,7:8));
        end
    end
else
    for i=1:size(dates_SMS,1)
        dates_SMS3{i}=strcat(dates_SMS2(i,1:6),'20',dates_SMS2(i,7:8));
    end
end

dates_SMS4=char(dates_SMS3);


part_1=str2double(dates_SMS4(1,1:2)); part_2=str2double(dates_SMS4(1,4:5));
part_3=str2double(dates_SMS4(1,7:10)); part_4=str2double(dates_cosmos3(1,1:2));
part_5=str2double(dates_cosmos3(1,4:5)); part_6=str2double(dates_cosmos3(1,7:10));
```

```
dates_SMS4_shift=(datenum(part_4,part_5,part_6)-datenum(part_1,part_2,part_3))+729;

clear dates_SMS dates_SMS2 dates_SMS3 i part_1 part_2 part_3 part_4 part_5 part_6;
```

```
headings={'date'    'temperature_[C]'    'rainfall_[mm]'    'VWC_[%]'    'sigma0_VH_[dB]'
'sigma0_VV_[dB]'      'SAR_penetratrion_depth_[cm]'      'TDT1_VWC_LEVEL2_MEAN_[%]'
'TDT2_VWC_LEVEL2_MEAN_[%] ' 'SMD_[mm/day]' 'SMS_[mm/day]' 'NDVI'};
```

```
cosmos_parameters_asc=zeros(size(dates_cosmos3,1),12);
cosmos_parameters_asc=[headings;num2cell(cosmos_parameters_asc)];
a=-5.3*10^-2; b=2.92*10^-2; c=-5.5*10^-4; d=4.3*10^-6; #Topp's model forumla #7


slope_angle=2.23; # mean in the buffer zone from 10m NextMap DTM
lambda=5.6; #wavelength of the SAR antenna [cm]
frequency=5.405; #C-band synthetic aperture radar frequency [GHz]
theta_asc=degtorad(37); theta_desc=degtorad(39); #incident angles at the COSMOS site from SNAP  [radians]


#fill the ascending matrix
h1 = waitbar(0,'Extracting COSMOS data, please wait ...');
count=2; #the first row is represented by the headings, so count must be =2!!!
for i=2:size(dates_cosmos3,1)   #original: for i=1:size(dates_cosmos3,1)
    cosmos_parameters_asc(count,1)=dates_cosmos3(i,:); #date we are considering
    cosmos_parameters_asc(count,2)=xlsread('CHOBH-2015-02-24-2018-08-27_buffer2-mean_median.xlsx','CHOBH-2015-02-24-2018-08-27',   strcat('F',num2str(i+6))); #F is the column of the mean air T [Celsius degrees]
    cosmos_parameters_asc(count,3)=xlsread('CHOBH-2015-02-24-2018-08-27_buffer2-mean_median.xlsx','CHOBH-2015-02-24-2018-08-27',   strcat('C',num2str(i+6))); #C is the column of the precipitation [mm]
    cosmos_parameters_asc(count,4)=xlsread('CHOBH-2015-02-24-2018-08-27_buffer2-mean_median.xlsx','CHOBH-2015-02-24-2018-08-27',   strcat('B',num2str(i+6))); #B is the column of the VWC [%]
    for i2=1:length(dates_asc3)
        if strfind(dates_cosmos3(i,:),dates_asc3(i2,:))==1; #we might do the correction for the incident angle following https://doi.org/10.3390/rs8110920
            cosmos_parameters_asc(count,5)=xlsread('CHOBH-2015-02-24-2018-08-27_buffer2-mean_median.xlsx','SAR_sigma0_asc', strcat('C',num2str(i2+2))); #C is the column of the median sigma0_VH [dB]
            cosmos_parameters_asc(count,6)=xlsread('CHOBH-2015-02-24-2018-08-27_buffer2-mean_median.xlsx','SAR_sigma0_asc', strcat('F',num2str(i2+2))); #F is the column of the median sigma0_VV [dB]
        end
    end
    if isempty(cosmos_parameters_asc{count,4})==0
    VWC=cosmos_parameters_asc{count,4};                 e=((nthroot(VWC-a,3))-(nthroot(b,2))-(nthroot(c,1))); #e, dielectric constant
    cosmos_parameters_asc(count,7)=((lambda*nthroot(e,2))/(2*pi*e));# SAR penetration depth [cm] from_Koyama_et_al.(2017)
    end
```

27

```
    cosmos_parameters_asc(count,8)=xlsread('CHOBH-2015-02-24-2018-08-27_buffer2-
mean_median.xlsx','CHOBH-2015-02-24-2018-08-27',strcat('O',num2str(i+6)));
#TDT1_VWC_LEVEL2_MEAN [%]
    cosmos_parameters_asc(count,9)=xlsread('CHOBH-2015-02-24-2018-08-27_buffer2-
mean_median.xlsx','CHOBH-2015-02-24-2018-08-27',strcat('Q',num2str(i+6)));
#TDT2_VWC_LEVEL2_MEAN [%]


cosmos_parameters_asc(count,10)=xlsread('ChobhamCommon_SMD_and_SMS.xlsx','Plot_SM
D',strcat('C',num2str(count+dates_SMS4_shift)));# SMD from P2S2 of Majdi Mansour
[mm/day] take the dates_SMS4_shift into account!!

cosmos_parameters_asc(count,11)=xlsread('ChobhamCommon_SMD_and_SMS.xlsx','SoilStora
ge_vs_VWC',strcat('C',num2str(count+dates_SMS4_shift)));# SMS from Majdi Mansour
[mm/day]
    #cosmos_parameters_asc(count,12)= NDVI extracted from Google Earth Engine; to be
developed
    count=count+1;
end
close(h1);


#replacing empty cells with NaN and 0 in the sigmas with NaN
clear i;
for i=2:size(cosmos_parameters_asc,1)
  for c=2:size(cosmos_parameters_asc,2)
    if c==5 | c==6 | c==12
      if cosmos_parameters_asc{i,c}==0
        cosmos_parameters_asc{i,c}=NaN;
      end
    end
    if isempty(cosmos_parameters_asc{i,c})==1
      cosmos_parameters_asc{i,c}=NaN;
    end
  end
end
save cosmos_parameters_asc
```

Output: cosmos_parameters_asc where information on the VWC from CRS and corresponding σ_0 are stored. cosmos_parameters_asc will be used in following script, Post_processing.m, which is calling other another script:

post_processing.m > raw_correlation.m

post_processing.m

#post processing
clear
load('C:\Users\alessn\Desktop\projects and proposals\KE_fellowship\Innovation Flexible Fund\COSMOS_data\ChobhamCommon_Reading\cosmos_parameters_asc')
place='ChobhamCommon'; SAR_dataset='asc'; input_data=cosmos_parameters_asc;
output_name=strcat(place,'_',SAR_dataset);

#next upgrade: extract the date automatically!
startdate=datenum('24-feb-2015'); enddate=datenum('27-aug-2018');
xData=[startdate:1:enddate]; # for ChobhamCommon
#startdate=datenum('1-jan-2016'); enddate=datenum('27-aug-2018');
xData=[startdate:1:enddate]; #HollinHill

#add NDVI values in cosmos_parameters_asc, next upgrade: take NDVI values manually
dateFormat = 20; NDVI=cell2mat(input_data(2:end,12));
scatter(xData,NDVI); datetick(dateFormat); hold on;
NDVI2=NDVI(~isnan(NDVI)); xData2=xData(~isnan(NDVI)); xData3=[1:1:size(xData2,2)];

#fitting of NDVI throught the COSMOS period
NDVI_interp2=interp1(xData2,NDVI2,xData);
plot(xData,NDVI_interp2,'-'); legend({'NDVI measured','NDVI interpolated'});
saveas(gcf,strcat('NDVI_interpolation'),'jpg');
close(gcf);

[AX H1 H2]=plotyy(xData,cell2mat(input_data(2:end,5)),xData,NDVI_interp2,'scatter'); #VH
hold(AX(2)); scatter(xData,cell2mat(input_data(2:end,6)),'d','MarkerEdgeColor',[0 .5 .5]); #VV
dateFormat = 20; datetick(AX(1),dateFormat); datetick(AX(2),dateFormat); title('NDVI');
legend({'VH [dB]','VV [dB]', 'NDVI_interp'});
saveas(gcf,strcat(output_name,'_','NDVI_interpolation_vs_SAR'),'jpg'); close(gcf);

#correlation coefficient with and without weights for the same day acquisitions
NDVI_threshold=0.5; SMS_threshold=50;
[corrcoef_best,VWC_weighted,VH_weighted,VV_weighted]=same_day_correlation(input_data, output_name,NDVI_interp2,NDVI_threshold,SMS_threshold) #VH first and VV second without and with weights

#correlation coefficient for average of 2, 3, 4 and 5 days with or without NDVI and SMS filters
[corrcoef_best_2days,corrcoef_best_3days,corrcoef_best_4days,corrcoef_best_5days,...
corrcoef_best_2days_weighted,corrcoef_best_3days_weighted,corrcoef_best_4days_weighted,c orrcoef_best_5days_weighted]=averaged_days(input_data,output_name,VH_weighted,VV_weig hted)

#correlation coefficient for delay of 2, 3, 4 and 5 days with or without NDVI and SMS filters
[corrcoef_best_1_day_delay,corrcoef_best_2_days_delay,corrcoef_best_3_days_delay,corrcoef_best_4_days_delay,corrcoef_best_5_days_delay,...
corrcoef_best_1_day_delay_weighted,corrcoef_best_2_days_delay_weighted,corrcoef_best_3_days_delay_weighted,corrcoef_best_4_days_delay_weighted,corrcoef_best_5_days_delay_weighted]...
=delayed_days(input_data,output_name,VH_weighted,VV_weighted)

#merge all correlation coefficient in one array to take the best
all_corr_coefficient=[corrcoef_best';corrcoef_best_2days';corrcoef_best_3days';...
corrcoef_best_4days';corrcoef_best_5days';corrcoef_best_2days_weighted';corrcoef_best_3days_weighted';...
corrcoef_best_4days_weighted';corrcoef_best_5days_weighted';...
corrcoef_best_1_day_delay';corrcoef_best_2_days_delay';corrcoef_best_3_days_delay';corrcoef_best_4_days_delay';corrcoef_best_5_days_delay';...
corrcoef_best_1_day_delay_weighted';corrcoef_best_2_days_delay_weighted';corrcoef_best_3_days_delay_weighted';corrcoef_best_4_days_delay_weighted';corrcoef_best_5_days_delay_weighted'];

same_day_correlation.m

*function
[corrcoef_best,VWC_weighted,VH_weighted,VV_weighted]=same_day_correlation(input_data,output_name,NDVI_interp2,NDVI_threshold,SMS_threshold);*

#choose the best correlation with no weights
corrcoef_VWC_VH=corrcoef(cell2mat(input_data(2:end,4)),cell2mat(input_data(2:end,5)));
#corr coeff between VWC and VH (median), sum(~isnan(cell2mat(input_data(2:end,5))))
corrcoef_VWC_VV=corrcoef(cell2mat(input_data(2:end,4)),cell2mat(input_data(2:end,6)));
#corr coeff between VWC and VV (median)

#just analyse the correlation coefficient between CRS and sigma0 filtered by NDVI
VWC_weighted=cell2mat(input_data(2:end,4)); VH_weighted=cell2mat(input_data(2:end,5));
VV_weighted=cell2mat(input_data(2:end,6));
VWC_weighted(NDVI_interp2<=(NDVI_threshold)) = NaN;
VH_weighted(NDVI_interp2<=(NDVI_threshold)) = NaN;
VV_weighted(NDVI_interp2<=(NDVI_threshold)) = NaN;
corrcoef_VWC_VH_weighted=corrcoef(VWC_weighted,VH_weighted); #corr coeff between VWC and VH (median)
corrcoef_VWC_VV_weighted=corrcoef(VWC_weighted,VV_weighted); #corr coeff between VWC and VH (median)

corrcoef_best=[corrcoef_VWC_VH,corrcoef_VWC_VV,corrcoef_VWC_VH_weighted,corrcoef_VWC_VV_weighted]; corrcoef_best2=max(corrcoef_best);
corrcoef_best_index=find(corrcoef_best==corrcoef_best2);

averaged_days.m

function
[corrcoef_best_2days,corrcoef_best_3days,corrcoef_best_4days,corrcoef_best_5days,...
corrcoef_best_2days_weighted,corrcoef_best_3days_weighted,corrcoef_best_4days_weighted,c
orrcoef_best_5days_weighted]=averaged_days(input_data,output_name,VH_weighted,VV_weig
hted)

VWC_2successive_days_average=[]; #TDT1_2successive_days_average=[];
TDT2_2successive_days_average=[];
#find correlation sigma0 with the average of future VWC (up to 5 days) measurements

#2 successive days average
for i=2:length(input_data)-1

VWC_2successive_days_average(i,1)=(cell2mat(input_data(i,4))+cell2mat(input_data(i+1,4)))/
2;
end

#3 successive days average
for i=2:length(input_data)-2

VWC_3successive_days_average(i,1)=(cell2mat(input_data(i,4))+cell2mat(input_data(i+1,4))+
cell2mat(input_data(i+2,4)))/3;#VWC
end

#4 successive days average
for i=2:length(input_data)-3

VWC_4successive_days_average(i,1)=(cell2mat(input_data(i,4))+cell2mat(input_data(i+1,4))+
cell2mat(input_data(i+2,4))+cell2mat(input_data(i+3,4)))/4;#VWC   #M = mean(A,'omitnan')
to exclude NaN values
end

#5 successive days average
for i=2:length(input_data)-4

VWC_5successive_days_average(i,1)=(cell2mat(input_data(i,4))+cell2mat(input_data(i+1,4))+
cell2mat(input_data(i+2,4))+cell2mat(input_data(i+3,4))+cell2mat(input_data(i+4,4)))/5;#VW
C   #M = mean(A,'omitnan') to exclude NaN values
end

#2days corr coeff without weights
corrcoef_VWC_VH_2days=corrcoef(VWC_2successive_days_average,cell2mat(input_data(2:en
d,5))); #corr coeff between VWC and VH
corrcoef_VWC_VV_2days=corrcoef(VWC_2successive_days_average,cell2mat(input_data(2:en
d,6))); #corr coeff between VWC and VV
corrcoef_best_2days=[corrcoef_VWC_VH_2days,corrcoef_VWC_VV_2days];

#3days corr coeff without weights
corrcoef_VWC_VH_3days=corrcoef(VWC_3successive_days_average,cell2mat(input_data(2:en
d-1,5))); #corr coeff between VWC and VH

```
corrcoef_VWC_VV_3days=corrcoef(VWC_3successive_days_average,cell2mat(input_data(2:end-1,6))); #corr coeff between VWC and VV
corrcoef_best_3days=[corrcoef_VWC_VH_3days,corrcoef_VWC_VV_3days];

#4days corr coeff without weights
corrcoef_VWC_VH_4days=corrcoef(VWC_4successive_days_average,cell2mat(input_data(2:end-2,5))); #corr coeff between VWC and VH
corrcoef_VWC_VV_4days=corrcoef(VWC_4successive_days_average,cell2mat(input_data(2:end-2,6))); #corr coeff between VWC and VV
corrcoef_best_4days=[corrcoef_VWC_VH_4days,corrcoef_VWC_VV_4days];

#5days corr coeff without weights
corrcoef_VWC_VH_5days=corrcoef(VWC_5successive_days_average,cell2mat(input_data(2:end-3,5))); #corr coeff between VWC and VH
corrcoef_VWC_VV_5days=corrcoef(VWC_5successive_days_average,cell2mat(input_data(2:end-3,6))); #corr coeff between VWC and VV
corrcoef_best_5days=[corrcoef_VWC_VH_5days,corrcoef_VWC_VV_5days];

#2days corr coeff with weights
corrcoef_VWC_VH_2days_weighted=corrcoef(VWC_2successive_days_average,VH_weighted); #corr coeff between VWC and VH
corrcoef_VWC_VV_2days_weighted=corrcoef(VWC_2successive_days_average,VV_weighted); #corr coeff between VWC and VV
corrcoef_best_2days_weighted=[corrcoef_VWC_VH_2days_weighted,corrcoef_VWC_VV_2days_weighted];

#3days corr coeff with weights
corrcoef_VWC_VH_3days_weighted=corrcoef(VWC_3successive_days_average,VH_weighted(1:end-1)); #corr coeff between VWC and VH
corrcoef_VWC_VV_3days_weighted=corrcoef(VWC_3successive_days_average,VV_weighted(1:end-1)); #corr coeff between VWC and VV
corrcoef_best_3days_weighted=[corrcoef_VWC_VH_3days_weighted,corrcoef_VWC_VV_3days_weighted];

#4days_weighted corr coeff with weights
corrcoef_VWC_VH_4days_weighted=corrcoef(VWC_4successive_days_average,VH_weighted(1:end-2)); #corr coeff between VWC and VH
corrcoef_VWC_VV_4days_weighted=corrcoef(VWC_4successive_days_average,VV_weighted(1:end-2)); #corr coeff between VWC and VV
corrcoef_best_4days_weighted=[corrcoef_VWC_VH_4days_weighted,corrcoef_VWC_VV_4days_weighted];

#5days_weighted corr coeff with weights
corrcoef_VWC_VH_5days_weighted=corrcoef(VWC_5successive_days_average,VH_weighted(1:end-3)); #corr coeff between VWC and VH
corrcoef_VWC_VV_5days_weighted=corrcoef(VWC_5successive_days_average,VV_weighted(1:end-3)); #corr coeff between VWC and VV
corrcoef_best_5days_weighted=[corrcoef_VWC_VH_5days_weighted,corrcoef_VWC_VV_5days_weighted];
```

delayed_days.m

```
function
[corrcoef_best_1day_delay,corrcoef_best_2days_delay,corrcoef_best_3days_delay,corrcoef_best_4days_delay,corrcoef_best_5days_delay,...
corrcoef_best_1day_delay_weighted,corrcoef_best_2days_delay_weighted,corrcoef_best_3days_delay_weighted,corrcoef_best_4days_delay_weighted,corrcoef_best_5days_delay_weighted]...
=delayed_days(input_data,output_name,VH_weighted,VV_weighted)


VWC_1_day_delay=[];
for i=2:length(input_data)-1
    VWC_1_day_delay(i,1)=cell2mat(input_data(i+1,4));
end


VWC_2_days_delay=[];
for i=2:length(input_data)-2
    VWC_2_days_delay(i,1)=cell2mat(input_data(i+2,4));
end


VWC_3_days_delay=[];
for i=2:length(input_data)-3
    VWC_3_days_delay(i,1)=cell2mat(input_data(i+3,4));
end


VWC_4_days_delay=[];
for i=2:length(input_data)-4
    VWC_4_days_delay(i,1)=cell2mat(input_data(i+4,4));
end


VWC_5_days_delay=[]; TDT1_5_days_delay=[]; TDT2_5_days_delay=[];
for i=2:length(input_data)-5
    VWC_5_days_delay(i,1)=cell2mat(input_data(i+5,4));
end
```

```
#1day_delay corr coeff without filters
corrcoef_VWC_VH_1day_delay=corrcoef(VWC_1_day_delay,cell2mat(input_data(2:end,5))); #corr coeff between VWC and VH
corrcoef_VWC_VV_1day_delay=corrcoef(VWC_1_day_delay,cell2mat(input_data(2:end,6))); #corr coeff between VWC and VV
corrcoef_best_1day_delay=[corrcoef_VWC_VH_1day_delay,corrcoef_VWC_VV_1day_delay];

#1day_delay corr coeff with filters
corrcoef_VWC_VH_1day_delay_weighted=corrcoef(VWC_1_day_delay,VH_weighted); #corr coeff between VWC and VH
corrcoef_VWC_VV_1day_delay_weighted=corrcoef(VWC_1_day_delay,VV_weighted); #corr coeff between VWC and VV
corrcoef_best_1day_delay_weighted=[corrcoef_VWC_VH_1day_delay_weighted,corrcoef_VWC_VV_1day_delay_weighted];

#2days_delay corr coeff without filters
corrcoef_VWC_VH_2days_delay=corrcoef(VWC_2_days_delay,cell2mat(input_data(2:end-1,5))); #corr coeff between VWC and VH
corrcoef_VWC_VV_2days_delay=corrcoef(VWC_2_days_delay,cell2mat(input_data(2:end-1,6))); #corr coeff between VWC and VV
```

corrcoef_best_2days_delay=[corrcoef_VWC_VH_2days_delay,corrcoef_VWC_VV_2days_delay];

corrcoef_VWC_VH_2days_delay_weighted=corrcoef(VWC_2_days_delay,VH_weighted(1:end-1,1)); #corr coeff between VWC and VH
corrcoef_VWC_VV_2days_delay_weighted=corrcoef(VWC_2_days_delay,VV_weighted(1:end-1,1)); #corr coeff between VWC and VV
corrcoef_best_2days_delay_weighted=[corrcoef_VWC_VH_2days_delay_weighted,corrcoef_VWC_VV_2days_delay_weighted];

corrcoef_VWC_VH_3days_delay=corrcoef(VWC_3_days_delay,cell2mat(input_data(2:end-2,5))); #corr coeff between VWC and VH
corrcoef_VWC_VV_3days_delay=corrcoef(VWC_3_days_delay,cell2mat(input_data(2:end-2,6))); #corr coeff between VWC and VV
corrcoef_best_3days_delay=[corrcoef_VWC_VH_2days_delay,corrcoef_VWC_VV_3days_delay];

corrcoef_VWC_VH_3days_delay_weighted=corrcoef(VWC_3_days_delay,VH_weighted(1:end-2,1)); #corr coeff between VWC and VH
corrcoef_VWC_VV_3days_delay_weighted=corrcoef(VWC_3_days_delay,VV_weighted(1:end-2,1)); #corr coeff between VWC and VV
corrcoef_best_3days_delay_weighted=[corrcoef_VWC_VH_3days_delay_weighted,corrcoef_VWC_VV_3days_delay_weighted];

corrcoef_VWC_VH_4days_delay=corrcoef(VWC_4_days_delay,cell2mat(input_data(2:end-3,5))); #corr coeff between VWC and VH
corrcoef_VWC_VV_4days_delay=corrcoef(VWC_4_days_delay,cell2mat(input_data(2:end-3,6))); #corr coeff between VWC and VV
corrcoef_best_4days_delay=[corrcoef_VWC_VH_4days_delay,corrcoef_VWC_VV_4days_delay];

corrcoef_VWC_VH_4days_delay_weighted=corrcoef(VWC_4_days_delay,VH_weighted(1:end-3,1)); #corr coeff between VWC and VH
corrcoef_VWC_VV_4days_delay_weighted=corrcoef(VWC_4_days_delay,VV_weighted(1:end-3,1)); #corr coeff between VWC and VV
corrcoef_best_4days_delay_weighted=[corrcoef_VWC_VH_4days_delay_weighted,corrcoef_VWC_VV_4days_delay_weighted];

corrcoef_VWC_VH_5days_delay=corrcoef(VWC_5_days_delay,cell2mat(input_data(2:end-4,5))); #corr coeff between VWC and VH
corrcoef_VWC_VV_5days_delay=corrcoef(VWC_5_days_delay,cell2mat(input_data(2:end-4,6))); #corr coeff between VWC and VV
corrcoef_best_5days_delay=[corrcoef_VWC_VH_5days_delay,corrcoef_VWC_VV_5days_delay];

#5days_delay corr coeff with filters

corrcoef_VWC_VH_5days_delay_weighted=corrcoef(VWC_5_days_delay,VH_weighted(1:end-4,1)); #corr coeff between VWC and VH

corrcoef_VWC_VV_5days_delay_weighted=corrcoef(VWC_5_days_delay,VV_weighted(1:end-4,1)); #corr coeff between VWC and VV

corrcoef_best_5days_delay_weighted=[corrcoef_VWC_VH_5days_delay_weighted,corrcoef_VWC_VV_5days_delay_weighted];

Appendix 2

The fourty combinations for Chobham Common are reported in Table A1 for the ascending geometry and Table A2 for the descending geometry.

Table A1 – Correlation coefficients between VWC and σ_0 for the ascending geometry in Chobham Common. The column 'threshold' refers to the eventual application of the NDVI and SMS filters. A filter of ≤0.6 for NDVI and ≤50 mm/day for SMS have been applied.

same day	
VWC vs σ0 (VH)	*VWC vs σ0 (VV)*
0.53	0.58

same day with NDVI & SMS thresholds	
VWC vs σ0 (VH)	*VWC vs σ0 (VV)*
0.56	0.69

with delays after the satellite acquisition			
thresholds	*delay [day]*	*VWC vs σ0 (VH)*	*VWC vs σ0 (VV)*
N	1	0.52	0.58
N	2	0.5	0.57
N	3	0.5	0.55
N	4	0.45	0.52
N	5	0.48	0.56
Y	1	0.56	0.69
Y	2	0.54	0.71
Y	3	0.53	0.68
Y	4	0.49	0.66
Y	5	0.61	0.74

with average of VWC-CRS measurements following the satellite acquisition			
thresholds	*average [day]*	*VWC vs σ0 (VH)*	*VWC vs σ0 (VV)*
N	2	0.53	0.61
N	3	0.53	0.61
N	4	0.53	0.6
N	5	0.52	0.59
Y	2	0.59	0.736
Y	3	0.58	0.738
Y	4	0.58	0.731
Y	5	0.56	0.72

Table A2 – Correlation coefficients between VWC and σ₀ for the descending geometry in Chobham Common. The column 'threshold' refers to the eventual application of the NDVI and SMS filters. A filter of ≤0.5 for NDVI and ≤50 mm/day for SMS have been applied.

same day

VWC vs $\sigma 0$ (VH)	VWC vs $\sigma 0$ (VV)
0.26	0.51

same day with NDVI & SMS thresholds

VWC vs $\sigma 0$ (VH)	VWC vs $\sigma 0$ (VV)
0.2	0.54

with delays after the satellite acquisition

thresholds	delay [day]	VWC vs $\sigma 0$ (VH)	VWC vs $\sigma 0$ (VV)
N	1	0.26	0.51
N	2	0.22	0.46
N	3	0.22	0.45
N	4	0.21	0.44
N	5	0.23	0.45
Y	1	0.2	0.54
Y	2	0.16	0.5
Y	3	0.16	0.48
Y	4	0.16	0.44
Y	5	0.19	0.48

with average of VWC-CRS measurements following the satellite acquisition

thresholds	average [day]	VWC vs $\sigma 0$ (VH)	VWC vs $\sigma 0$ (VV)
N	2	0.26	0.51
N	3	0.25	0.5
N	4	0.25	0.49
N	5	0.24	0.49
Y	2	0.21	0.55
Y	3	0.2	0.54
Y	4	0.19	0.53
Y	5	0.19	0.52

The fourty combinations for Hollin Hill are reported in Table A3 for the ascending geometry and Table A4 for the descending geometry.

Table A3 – Correlation coefficients between VWC and σ₀ for the ascending geometry in Hollin Hill. The column 'threshold' refers to the eventual application of the NDVI and SMS filters. A filter of ≤0.5 for NDVI and ≤50 mm/day for SMS have been applied.

same day	
VWC vs σ0 (VH)	*VWC vs σ0 (VV)*
0.39	0.5

same day with NDVI & SMS thresholds	
VWC vs σ0 (VH)	*VWC vs σ0 (VV)*
0.38	0.45

with delays after the satellite acquisition

thresholds	*delay [day]*	*VWC vs σ0 (VH)*	*VWC vs σ0 (VV)*
N	1	0.31	0.41
N	2	0.3	0.47
N	3	0.3	0.39
N	4	0.23	0.34
N	5	0.23	0.44
Y	1	0.38	0.44
Y	2	0.32	0.48
Y	3	0.28	0.44
Y	4	0.25	0.42
Y	5	0.24	0.5

with average of VWC-CRS measurements following the satellite acquisition

thresholds	*average [day]*	*VWC vs σ0 (VH)*	*VWC vs σ0 (VV)*
N	2	0.35	0.45
N	3	0.38	0.46
N	4	0.4	0.46
N	5	0.36	0.41
Y	2	0.43	0.54
Y	3	0.46	0.57
Y	4	0.51	0.58
Y	5	0.47	0.54

Table A4 – Correlation coefficients between VWC and σ₀ for the descending geometry in Hollin Hill. The column 'threshold' refers to the eventual application of the NDVI and SMS filters. A filter of ≤0.4 for NDVI and ≤50 mm/day for SMS have been applied.

same day

VWC vs σ0 (VH)	VWC vs σ0 (VV)
0.3	0.32

same day with NDVI & SMS thresholds

VWC vs σ0 (VH)	VWC vs σ0 (VV)
0.2	0.17

with delays after the satellite acquisition

thresholds	delay [day]	VWC vs σ0 (VH)	VWC vs σ0 (VV)
N	1	0.3	0.32
N	2	0.28	0.35
N	3	0.28	0.29
N	4	0.22	0.29
N	5	0.17	0.27
Y	1	0.2	0.13
Y	2	0.22	0.2
Y	3	0.22	0.17
Y	4	0.18	0.16
Y	5	0.15	0.14

with average of VWC-CRS measurements following the satellite acquisition

thresholds	average [day]	VWC vs σ0 (VH)	VWC vs σ0 (VV)
N	2	0.29	0.36
N	3	0.3	0.37
N	4	0.33	0.38
N	5	0.35	0.39
Y	2	0.18	0.19
Y	3	0.2	0.19
Y	4	0.28	0.19
Y	5	0.26	0.15

References

ALEXAKIS, D.D., MEXIS, F.D.K., VOZINAKI, A.E.K., DALIAKOPOULOS, I.N. and TSANIS, I.K., 2017. SOIL MOISTURE CONTENT ESTIMATION BASED ON SENTINEL-1 AND AUXILIARY EARTH OBSERVATION PRODUCTS. A HYDROLOGICAL APPROACH. SENSORS, 17(6), P.1455. HTTPS://DOI.ORG/10.3390/S17061455

BAATZ, R., BOGENA, H.R., HENDRICKS FRANSSEN, H.-J., HUISMAN, J.A., QU, W., MONTZKA, C., and VEREECKEN, H., 2014. CALIBRATION OF A CATCHMENT SCALE COSMIC-RAY PROBE NETWORK: A COMPARISON OF THREE PARAMETERIZATION METHODS, J. HYDROL., 516, 231–244. HTTPS://DOI.ORG/10.1016/J.JHYDROL.2014.02.026

BAGHDADI, N., HOLAH, N. and ZRIBI, M., 2006. SOIL MOISTURE ESTIMATION USING MULTI‐INCIDENCE AND MULTI‐POLARIZATION ASAR DATA. INTERNATIONAL JOURNAL OF REMOTE SENSING, 27(10), PP.1907-1920. HTTPS://DOI.ORG/10.1080/01431160500239032

BAGHDADI, N., CHOKER, M., ZRIBI, M., HAJJ, M.E., PALOSCIA, S., VERHOEST, N.E., LIEVENS, H., BAUP, F. and MATTIA, F., 2016. A NEW EMPIRICAL MODEL FOR RADAR SCATTERING FROM BARE SOIL SURFACES. REMOTE SENSING, 8(11), P.920. HTTPS://DOI.ORG/10.3390/RS8110920

BAUER- MARSCHALLINGER, B., PAULIK, C., HOCHSTÖGER, S., MISTELBAUER, T., MODANESI, S., CIABATTA, L., MASSARI, C., BROCCA, L. and WAGNER, W. 2018. SOIL MOISTURE FROM FUSION OF SCATTEROMETER AND SAR: CLOSING THE SCALE GAP WITH TEMPORAL FILTERING. REMOTE SENSING, 10(7), P.1030. HTTPS://DOI.ORG/10.3390/RS10071030

BOORMAN, D.B., HOLLIST, J.M. AND LILLY, A. 1995. HYDROGEOLOGY OF SOIL TYPES: A HYDROLOGICALLY-BASED CLASSIFICATION OF THE SOILS OF THE UNITED KINGDOM. INSTITUTE OF HYDROLOGY REPORT NO. 126. WALLINGFORD, UK.

CEH, 2018. COSMOS-UK USER GUIDE - USERS' GUIDE TO SITES, INSTRUMENTS AND AVAILABLE DATA. VERSION 2.10. AVAILABLE AT HTTPS://COSMOS.CEH.AC.UK/SITES/DEFAULT/FILES/COSMOS-UK%20USER%20GUIDE%20V2.10.PDF (ACCESSED ON 4/5/2019)

CHEN, Y. and XU, H., 2014. COMPARISONS OF SPECKLE NOISE FILTERING METHODS ON INTERFEROMETRIC SYNTHETIC APERTURE RADAR IMAGES. JOURNAL OF COMPUTERS, 9(4), 908-915, HTTPS://DOI.ORG/10.4304/JCP.9.4.908-915

CIGNA, F., BATESON, L.B., JORDAN, C.J. and DASHWOOD, C., 2014. SIMULATING SAR GEOMETRIC DISTORTIONS AND PREDICTING PERSISTENT SCATTERER DENSITIES FOR ERS-1/2 AND ENVISAT C-BAND SAR AND INSAR APPLICATIONS: NATIONWIDE FEASIBILITY ASSESSMENT TO MONITOR THE LANDMASS OF GREAT BRITAIN WITH SAR IMAGERY. REMOTE SENSING OF ENVIRONMENT, 152, PP.441-466. HTTPS://DOI.ORG/10.1016/J.RSE.2014.06.025

DAS, K. and PAUL, P.K., 2015. SOIL MOISTURE RETRIEVAL MODEL BY USING RISAT-1, C-BAND DATA IN TROPICAL DRY AND SUB-HUMID ZONE OF BANKURA DISTRICT OF INDIA. THE EGYPTIAN JOURNAL OF REMOTE SENSING AND SPACE SCIENCE, 18(2), 297-310. HTTPS://DOI.ORG/10.1016/J.EJRS.2015.09.004

DE JEU, R. and DORIGO, W. ON THE IMPORTANCE OF SATELLITE OBSERVED SOIL MOISTURE. INT. J. APPL. EARTH OBS. GEOINF. 2016, 45, 107–109. HTTPS://DOI.ORG/10.1016/J.JAG.2015.10.007

DE ZAN, F. and GUARNIERI, A. M. 2006. TOPSAR: TERRAIN OBSERVATION BY PROGRESSIVE SCANS. GEOSCIENCE AND REMOTE SENSING, IEEE TRANSACTIONS ON, 44(9), 2352–2360. HTTPS://DOI.ORG/10.1109/TGRS.2006.873853

ESA, 2016. SENTINEL-1 PRODUCT DEFINITION. AVAILABLE AT HTTPS://SENTINEL.ESA.INT/DOCUMENTS/247904/1877131/SENTINEL-1-PRODUCT-DEFINITION [ACCESSED ON 10/12/2019]

EVANS, J.G., WARD, H.C., BLAKE, J.R., HEWITT, E.J., MORRISON, R., FRY, M., BALL, L.A., DOUGHTY, L.C., LIBRE, J.W., HITT, O.E. and RYLETT, D., 2016. SOIL WATER CONTENT IN SOUTHERN ENGLAND DERIVED FROM A COSMIC-RAY SOIL MOISTURE OBSERVING SYSTEM–COSMOS-UK. HYDROLOGICAL PROCESSES, 30(26), PP.4987-4999. HTTPS://DOI.ORG/10.1002/HYP.10929

GRIFFITHS, J., YOUNG, A.R. and KELLER, V. 2006. MODEL SCHEME FOR REPRESENTING RAINFALL INTERCEPTION AND SOIL MOISTURE. 674 ENVIRONMENT AGENCY ENVIRONMENT AGENCY R & D PROJECT W6‐101 CONTINUOUS ESTIMATION OF RIVER FLOWS (CERF).

GRIFFITHS, J., KELLER, V., MORRIS, D. AND YOUNG, A.R. 2008. CONTINUOUS ESTIMATION OF RIVER FLOWS (CERF), ENVIRONMENT AGENCY REPORT SC030240. BRISTOL, UK.

JACKSON, C.R. and SPINK, A.E.F., 2004. USER'S MANUAL FOR THE GROUNDWATER FLOW MODEL ZOOMQ3D. NOTTINGHAM, UK, BRITISH GEOLOGICAL SURVEY, 107PP, IR/04/140. (UNPUBLISHED)

JIANG, Z., HUETE, A.R., CHEN, J., CHEN, Y., LI, J., YAN, G. and ZHANG, X., 2006. ANALYSIS OF NDVI AND SCALED DIFFERENCE VEGETATION INDEX RETRIEVALS OF VEGETATION FRACTION. REMOTE SENSING OF ENVIRONMENT, 101(3), PP.366-378. HTTPS://DOI.ORG/10.1016/J.RSE.2006.01.003

KOYAMA, C.N., LIU, H., TAKAHASHI, K., SHIMADA, M., WATANABE, M., KHUUT, T. and SATO, M., 2017. IN-SITU MEASUREMENT OF SOIL PERMITTIVITY AT VARIOUS DEPTHS FOR THE CALIBRATION AND VALIDATION OF LOW-FREQUENCY SAR SOIL MOISTURE MODELS BY USING GPR. REMOTE SENSING, 9(6), P.580. HTTPS://DOI.ORG/10.3390/RS9060580

MANSOUR, M.M. and HUGHES, A.G. 2004. USER'S MANUAL FOR THE DISTRIBUTED RECHARGE MODEL ZOODRM. BRITISH GEOLOGICAL SURVEY, 61PP. (IR/04/150) (UNPUBLISHED)

MANSOUR, M.M. WANG, L., WHITEMAN, M. and HUGHES, A.G. 2018. ESTIMATION OF SPATIALLY DISTRIBUTED GROUNDWATER POTENTIAL RECHARGE FOR THE UNIRED KINGDOM. QUARTERLY JOURNAL OF ENGINEERING GEOLOGY AND HYDROGEOLOGY, 51 (2). 247-263. HTTPS://DOI.ORG/10.1144/QJEGH2017-051

MetOffice, 2018. Summer 2018. Available at:
https://www.metoffice.gov.uk/binaries/content/assets/metofficegovuk/pdf/weather/learn-about/uk-past-events/interesting/2018/summer-2018---met-office.pdf [accessed on 7/2/2020]

McCarthy, M., Christidis, N., Dunstone, N., Fereday, D., Kay, G., Klein-Tank, A., LoweJ., Petch, J., Scaife and A., Stott, P., 2019. Drivers of the UK summer heatwave of 2018. Special Issue: Heatwave and Drought in 2018, 74(11). https://doi.org/10.1002/wea.3628

Natural Environment Research Council (NERC) 2000. Countryside Survey 2000 Module 7. Land Cover map 2000 Final Report. Centre for Ecology and Hydrology, Wallingford, UK.

Novellino, A., Cigna, F., Brahmi, M., Sowter, A., Bateson, L. and Marsh, S., 2017. Assessing the feasibility of a national InSAR ground deformation map of Great Britain with Sentinel-1. Geosciences, 7(2), p.19. https://doi.org/10.3390/geosciences7020019

Rowland, C., Morton, D., Carrasco T.L., McShane, G., O'Neil, A. and Wood, C., 2015. Land Cover Map 2015 (vector, GB). NERC Environmental Information Data Centre 12 April 2017, https://doi.org/10.5285/6c6c9203-7333-4d96-88ab-78925e7a4e73

Uhlemann, S., Chambers, J., Wilkinson, P., Maurer, H., Merritt, A., Meldrum, P., Kuras, O., Gunn, D., Smith, A. and Dijkstra, T., 2017. Four‐dimensional imaging of moisture dynamics during landslide reactivation. Journal of Geophysical Research: Earth Surface, 122(1), pp.398-418. https://doi.org/10.1002/2016JF003983

Verhoest, N.E., Lievens, H., Wagner, W., Álvarez-Mozos, J., Moran, M.S. and Mattia, F., 2008. On the soil roughness parameterization problem in soil moisture retrieval of bare surfaces from synthetic aperture radar. Sensors, 8(7), pp.4213-4248. https://doi.org/10.3390/s8074213

Wisler, C., O. and Brater, E., F.,1959. Hydrology. New York: John Wiley & Sons, Inc. ISBN 0 471 95634 1

Zreda, M., Desilets, D., Ferre, T.P.A. and Scott, R.L., 2008. Measuring soil moisture content non-invasively at intermediate spatial scale using cosmic-ray neutrons, Geophys. Res. Lett., 35, L21402. https://doi.org/10.1029/2008GL035655

Zreda M, Shuttleworth W, Zeng X, Zweck C, Desilets D, Franz T. and Rosolem R. 2012. COSMOS: the cosmic-ray soil moisture observing system. Hydrology and Earth System Sciences 16: 4079–4099.